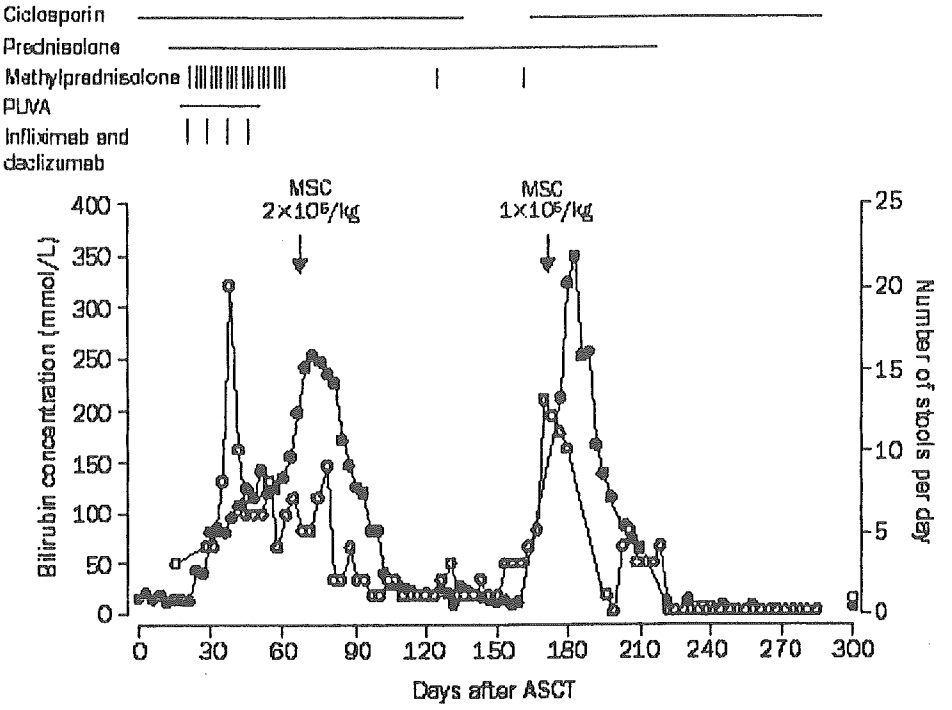

図6　臨床経過

難治性の肝と腸のGVHDに，母親(非ドナー)の骨髄から得られたMSCを2回投与したところ，血清ビリルビン(●)と便の回数(○)は著明に低下した。　(文献9より引用)

文　献

1) Pittenger MF, Martin BJ：Mesenchymal stem cells and their potential as cardiac therapeutics. Circ Res 95：9-20, 2004
2) Koc ON, et al：Allogeneic mesenchymal stem cell infusion for treatment of metachromatic leukodystrophy (MLD) and Hurler syndrome (MPS-IH). Bone Marrow Transplant 30：215-222, 2002
3) Horwitz EM, et al：Isolated allogeneic bone marrow-derived mesenchymal cells engraft and stimulate growth in children with osteogenesis imperfecta：Implications for cell therapy of bone.Proc Natl Acad Sci U S A 99：8932-8937, 2002
4) Koc ON, et al：Rapid hematopoietic recovery after coinfusion of autologous-blood stem cells and culture-expanded marrow mesenchymal stem cells in advanced breast cancer patients receiving high-dose chemotherapy. J Clin Oncol 18：307-316, 2000
5) Barker JN, et al：Transplantation of two partially HLA-matched umbilical cord blood units to enhance engraftment in adults with hematologic malignancy. Blood, 2004, 〔Epub ahead of print〕
6) Kim DW, et al：Cotransplantation of third-party mesenchymal stromal cells can alleviate single-donor predominance and increase engraftment from double cord transplantation. Blood 103：1941-1981, 2004
7) Maitra B,et al：Human mesenchymal stem cells support unrelated donor hematopoietic stem cells and suppress T-cell activation. Bone Marrow Transplant 33：597-604, 2004
8) Aggarwal S, Pittenger MF：Human mesenchymal stem cells modulate allogeneic immune cell responses. Blood, 2004 〔Epub ahead of print〕
9) O' Donoghue K, et al：Microchimerism in female bone marrow and bone decades after fetal mesenchymal stem-cell trafficking in pregnancy. Lancet 364：179-182, 2004

診断法をめぐる最近の進歩　5

Flow cytometry による MRD 検出

Detection of minimal residual disease using flow cytometry

Key point

◉AML, ALL, B 細胞性腫瘍の MRD を FCM を用いて検出することができる.

◉AML 細胞と ALL 細胞の検出における FCM の感度は約 0.1～0.01%と鋭敏である.

◉FCM で検出した MRD は AML と ALL の独立した予後因子である.

造血器腫瘍細胞の解析における FCM の役割

Flow cytometry(FCM)の原理は，細胞にレーザービームを照射し生じた散乱光や発色した螢光を検出する解析法であり，細胞の大きさ，細胞の密度，細胞が有している抗原の有無や強度を明らかにすることができる．均一な腫瘍性の細胞集団として増加する急性骨髄性白血病(AML)，急性リンパ性白血病(ALL)，悪性リンパ腫，多発性骨髄腫などの診断には FCM を用いた腫瘍細胞の解析が必須である．FCM の利点は迅速に結果が判明すること，再解析が可能であること，結果が定量的であることが上げられる．FCM で細胞を解析するにあたっては目的とする細胞集団を正常細胞集団から分離することが必要であり，種々のゲート法が考案されている．また，2 種類以上の螢光色素を標識したモノクローナル抗体を用いることによって細胞が発現する抗原の変化を詳細に解析することができ，multiparameter FCM や multidimensionl FCM とよばれている．FCM で得られた結果の解釈にあたっては正常造血幹細胞の分化に伴って発現する抗原の推移を理解する必要がある．

FCM を用いて微量の残存腫瘍細胞(MRD)を検出することができるが，MRD を検査するためには，①腫瘍細胞の細胞集団を正常細胞から分離すること，②腫瘍細胞が発現する抗原に変異が存在することの 2 つが必要である．①に関しては，AML や ALL が対象の場合には CD45 の発現強度と側方散乱の特性から白血病細胞集団を分離する CD45 ゲート法が用いられている[1](図 1)．通常，CD45 ゲート法に 3 種類の螢光色素を標識したモノクローナル抗体を組み合わせた 3-color FCM が主流である．②に関しては白血化に伴い AML と ALL の両者の約 90%に何らかの抗原変異を生じることが知られている(表 1)．CD45 ゲート法を用いた 3-color FCM の感度は約 0.1～0.01%と報告されており，顕微鏡による塗抹標本の観察や染色体分析に比べてはるかに鋭敏である．一方，白血病細胞にみられる抗原変異には画一的なパターンは存在しないので，頻度の高い抗原発現異常を検出できるよう抗体を組み合わせる必要がある．CD45 ゲート法では M3 を除く AML の白血病細胞は芽球領域に認められるが，ALL では腫瘍化に伴い CD45 の発現が低下し芽球領域よりも下の位置に存在する場合があることに注意を要する．

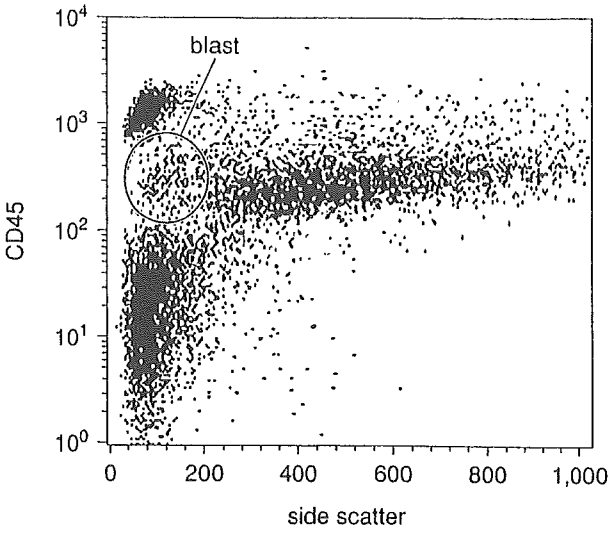

図 1　CD45 ゲート法で分離される芽球領域

当科での解析例を示す．AML-M0 の患者で，初診時の芽球は，$CD34^+$，$CD2^+$，$CD13^+$，$CD117^+$を呈した．寛解導入療法で形態学的には寛解と判定されたが，そのときの 3-color FCM では $CD34^+CD2^+$，$CD13^+$

サイドメモ

flow-FISH

螢光色素で標識したテロメア PNA プローブを用いてテロメアに対する FISH を行い，個々の細胞の螢光を FCM によって解析することができ，この方法は flow-FISH とよばれている．テロメアに対する FISH と細胞表面抗原に対する抗体で同時染色し，FCM で解析することによって特定の細胞集団におけるテロメア長の測定が可能である[11]．Flow-FISH によって造血器腫瘍の診断や治療にあらたな知見がもたらされることが期待される．

室井一男／自治医科大学附属病院輸血・細胞移植部
Kazuo MUROI

表 1　急性白血病でみられる抗原発現の異常

type of aberrancy	antigen
AML	
・expression of nonmyeloid-associated antigens	CD2+
	CD5+
	CD7+
	CD19+
	CD20+
	CD56+
・asynchronous expression	CD34+CD15+
	CD34+CD11b+
・overexpression	CD13++
	CD33++
	CD34++
・absence of myeloid-asscoiated antigen expression	CD33-
	CD11b-CD15-
B-ALL	
・expression of nonlymphoid-associated antigens	CD13+
	CD15+
	CD33+
・asynchronous expression	CD34+surface IgM+
	CD34+CD22+
・overexpression	CD10++
	CD34++
・absence of lymphoid-asscoiated antigen expression	CD19-
T-ALL	
・asynchronous expression	TdT+CD3+
	CD34+CD3+
・overexpression	CD7++

$CD2^+$，$CD117^+CD2^+$を示す白血病細胞の残存が認められ(図 2)，その後再発した．

急性白血病における FCM を用いた MRD の検出

AML や ALL の再発は，寛解到達後に残存している白血病細胞の増殖によって生じることが明らかとなっている．一般に寛解の判定は骨髄塗抹標本を検鏡し芽球が 5%未満のときになされる．より感度の高い FCM を用いた MRD の検出が AML の予後因子となることを示した報告がある．San Miguel ら[2]は寛解に到達した AML の MRD を FCM を用いて測定し，MRD のレベルによって 4 群(≧1%，1.0～0.1%，0.1～0.01%，<0.01%)に分かれること，MRD が多い群で有意に再発率が増加することを報告した(図 3-A)．多変量解析でも無再発生存に関与するもっとも強い独立因子は FCM の MRD レベルであった．最近，Kern ら[3]は，寛解導入時および地固め療法終了後の MRD を測定し，診断時からの白血病細胞の減少率を測定すると，減少率が高いほど無再発生存率が延長することを報告した．その他の報告でも，FCM で測定した MRD は独立した予後因子であるとの報告が多い．FCM を用いた MRD 検査の利点に，AML の病型や染色体異常(遺伝子異常)にとらわれないことがある．

AML と同様に ALL で MRD を検討した報告がある．Coustan-Smith ら[4]は，寛解導入療法終了後および地固め療法時の MRD を検査し，MRD が多いほど有意に再発が高いことを報告した(図 3-B)．同様な結果は他の報告からもみられ，多変量解析で MRD が独立した予後因子であることを示した報告もある．一方，化学療法後の骨髄の回復期には未熟な B 細胞の前駆細胞が一過性に増加し，形態上では残存している B 前駆細胞性白血病細胞と区別することが困難な場合がある．この細胞は hematogone とよばれている．hematogone は逸脱した抗原発現がみられないこと，分化に伴い B 細胞でみられる抗原が連続的に発現することから B 前駆細胞性白血病細胞と区別することが可能である[5]．

FCM を用いて MRD を検出するにあたって注意すべき点に抗原の変異がある[6]．再発時には AML および ALL の両者とも初診時に発現していた抗原が減弱したりあらたな抗原が発現したりする場合があるので，再発後の MRD 検出に FCM を用いる場合には再発時のマーカーを検査することが必要である．

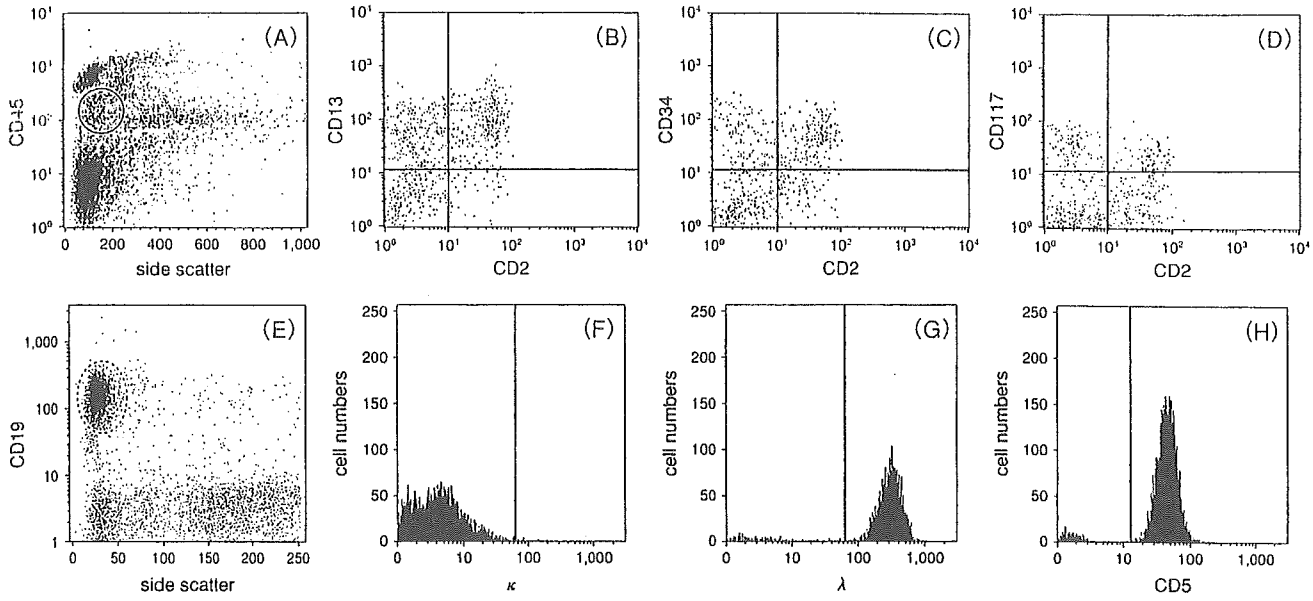

図 2　FCM を用いた MRD の検出

AML-M0 の症例で寛解と判定されたが，$CD13^+CD2^+$(B)，$CD34^+CD2^+$(C)，$CD117^+CD2^+$(D)を呈する白血病細胞の残存が認められた．B 細胞性リンパ腫の骨髄中の CD19 陽性細胞(E)に，κ^-(F)，λ^+(G)，$CD5^+$(H)のリンパ腫細胞が認められる．

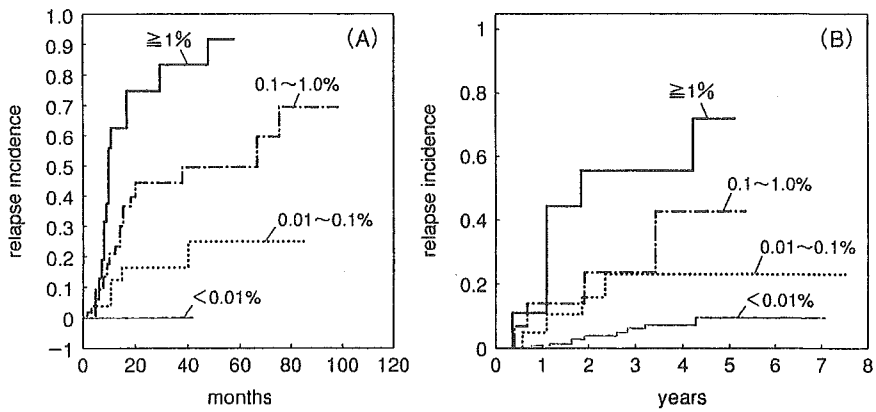

図 3　FCM で検出された MRD 量と再発との関係

A：AML[2]，B：ALL[4]．

成熟 B 細胞性腫瘍における FCM を用いた MRD の検出

B 細胞性リンパ腫はしばしば骨髄に浸潤するが，骨髄に浸潤すると臨床病期はIV期となり予後不良が示唆される．通常，骨髄浸潤の有無は骨髄生検や骨髄塗抹標本によってなされるが，FCM が B 細胞性リンパ腫の骨髄浸潤の判定に有用であるとの報告がある[7,8]．上述した CD45 ゲート法以外に，B 細胞性リンパ腫で発現する CD19 に着目し，CD19 ゲート[7]を用いて骨髄に浸潤している B 細胞性リンパ腫細胞を分離することができる(図 2)．急性白血病と異なり，B 細胞性リンパ腫では腫瘍化に伴う抗原発現の異常が少ないので，抗原発現異常からリンパ腫細胞を同定することは困難である．

一方，B 細胞の腫瘍化に伴い単一の免疫グロブリンが産生されるため，免疫グロブリンの軽鎖はκ鎖とλ鎖のどちらか一方の発現となる．正常骨髄 B 細胞おけるκ鎖とλ鎖の比は 0.5～3.0 の範囲とし，この範囲から逸脱した場合には腫瘍性の monoclonal B cell が存在するとしている報告が多い．B 細胞性リンパ腫が骨髄に浸潤する場合，局所的に骨髄に浸潤する場合があり，検体に浸潤部が含まれていない場合には FCM では偽陰性となることに注意を要する．また，急性白血病では FCM で検出した MRD が予後因子となるが，B 細胞性リンパ腫では FCM で検出した MRD が予後因子となるかは明らかではない．T 細胞性リンパ腫の場合には monoclonal TCR を FCM で検出することは困難であるので，FCM を用いた MRD 検出は有用ではない．

B 細胞性リンパ腫と同様に，多発性骨髄腫の MRD

もFCMで測定可能である．骨髄腫細胞は，CD38の発現が増強していること，しばしばCD56，CD117，CD138などの抗原発現異常がみられること，染色体にaneuploidyを生じることがあることから，これらの抗原発現異常やDNA含量と細胞質内の免疫グロブリンの軽鎖をFCMで測定することによって骨髄腫のMRDを検出することができる[9,10]．FCMを用いた骨髄腫のMRDの検出が造血幹細胞移植後の予後因子となるとの報告がある[9]．

おわりに

欧米からFCMを用いたMRD検出の報告はみられるが，わが国からの報告はきわめて少ない．FCMを用いたMRD検査は他の検査法に比べて優れた利点を有しており，わが国においてもFCMを用いたMRD検査が広く行われることが期待される．

*　　*　　*

文献

1) Stelzer, G. T. et al.：*Ann. NY. Acad. Sci. USA*, **677**：265-280, 1993.
2) San Miguel, J. F. et al.：*Blood*, **98**：1746-1751, 2001.
3) Kern, W. et al.：*Blood*, **104**：3078-3085, 2004.
4) Coustan-Smith, E. et al.：*Blood*, **96**：2691-2696, 2000.
5) McKenna, R. W. Et al.：*Leuk. Lymphoma.*, **45**：277-285, 2004.
6) Langebrake, C. et al.：*Cytometry B Clin. Cytom.*, **63**：1-9, 2005.
7) Kawano-Yamamoto, C. et al.：*Leuk. Lymphoma*, **43**：2133-2137, 2002.
8) Sah, S. P. et al.：*J. Clin. Pathol.*, **56**：129-132, 2003.
9) Andy, C. et al.：*Blood*, **100**：3095-3100, 2002.
10) Santonocito, A. M. et al.：*Leuk. Res.*, **28**：469-477, 2004.
11) Schmid, I. et al.：*Cytometry*, **49**：96-105, 2002.

Int. J. Cancer: **115**, 885–892 (2005)

Effect of differences in cancer cells and tumor growth sites on recruiting bone marrow-derived endothelial cells and myofibroblasts in cancer-induced stroma

Takafumi Sangai[1,2], Genichiro Ishii[1], Keiji Kodama[1], Shin'ichi Miyamoto[1], Yasuyuki Aoyagi[1], Takashi Ito[1], Junji Magae[3], Hiroki Sasaki[4], Takeshi Nagashima[2], Masaru Miyazaki[2] and Atsushi Ochiai[1]*

[1]*Pathology Division, National Cancer Center Research Institute East, Chiba, Japan*
[2]*Department of General Surgery, Graduate School of Medicine, Chiba University, Chiba, Japan*
[3]*Department of Biotechnology, Institute of Research and Innovation, Chiba, Japan*
[4]*Genetics Division, National Cancer Center Research Institute, Tokyo, Japan*

Cancer-stromal interaction is well known to play important roles during cancer progression. Recently we have demonstrated that bone marrow-derived vascular endothelial cells (BMD-VE) and myofibroblasts (BMD-MF) are recruited into the human pancreatic cancer cell line Capan-1 induced stroma. To assess the effect of the difference in cancer cell types on the recruitment of BMD-VE and BMD-MF, 10 kinds of human cancer cell line were implanted into the subcutaneous tissue of the immunodeficient mice transplanted with bone marrow of double-mutant mice (RAG-1−/− β-gal Tg or RAG-1−/− GFP Tg). The recruitment frequency of BMD-VE (%BMD-VE) and BMD-MF (%BMD-MF), and tumor-associated parameters [tumor volume (TV), microvessel density (MVD) and stromal proportion (%St)] were measured. The correlation among them was analyzed. Although %BMD-VE and %BMD-MF varied (from 0 to 21.6%, 0 to 29.6%, respectively), depending on the cancer cell line, both parameters were significantly correlated with %St ($p < 0.005$). Furthermore %BMD-VE and %BMD-MF also significantly correlated ($p < 0.005$). In order to assess the effect of tumor growth sites on the recruitment of the cells of interest, a human pancreatic cancer cell line, Capan-1, was transplanted into 5 different sites: subcutaneous tissue, peritoneum, liver, spleen and lung. Tumors in the subcutaneous tissue and peritoneum induced desmoplastic stroma (%St = 22.7%, 19.5%, respectively) and contained BMD-VE (%BMD-VE = 21.6%, 16.5% respectively) and BMD-MF (%BMD-MF = 29.6%, 24.5%, respectively), but weak stromal induction without recruitment of BMD-VE or -MF was observed in the tumors at of the liver, spleen and lung (%St = 9.7%, 9.1%, 5.4%, respectively). cDNA microarray analysis identified the 29 genes that expression was especially up- or down-regulated in the cell line that induced an abundant stromal reaction. However they did not encoded the molecules that were directly involved in stromal cell recruitment (chemokines), differentiation (cytokines) or proliferation (growth factors). These results indicate that the recruitment of BMD-VE and -MF is required for stromal formation during cancer progression and that the cancer microenvironment is important in stromal reaction and the recruitment of BMD-VE and -MF.

Key words: cancer-induced stroma; neovascularization; desmoplastic reaction; bone marrow-derived cells; endothelial cells; myofibroblasts

Invasive cancer tissue is composed of not only cancer cells but also various stromal cells: inflammatory cells, vascular cells and fibroblasts. It is well recognized that cancer-stromal interactions are critical in tumor growth and progression.[1–3] Pathological "neovascularization" and "desmoplastic reaction", *i.e.*, an increase in myofibroblasts and collagen fibers, frequently appear in the stroma of human invasive cancer tissue. Investigators including us have reported that the assessment of neovascularization and desmoplastic reaction is potentially useful for evaluating biological prognostic and predictive factors in human solid tumors.[4–6] Weidner *et al.*[7] reported a significant correlation between the degrees of microvessel density (MVD) and the probability of metastasis in invasive breast cancer patients.[7] In another study with invasive ductal carcinoma of the breast, the presence of a fibrotic focus defined as a dense fibroblast proliferation is closely associated with c-erbB-2 or p53 protein expression and high proliferative activity of the tumor cells and is the most useful independent parameter to predict patient outcome.[8] These data indicate that the cancer-stromal interaction plays important roles in cancer progression.

Among cancer stromal cells, inflammatory cells and vascular endothelial cells have been reported to be BM-derived and involved in tumor progression.[9–12] Concerning the origin of the fibroblasts, the increase of cancer-induced fibroblasts is believed to be a local event and results from clonal expansion, or alternatively the fibroblasts originate from other sites and migrate into the cancer tissue. Recently, we demonstrated that around 40% of myofibroblast were recruited from BM and had significant proliferative activity in the subcutaneously transplanted tumor of a human pancreatic cancer cell line.[13] Since myofibroblast has been reported to play important roles in angiogenesis, cancer cell survival, proliferation and invasion,[14–18] "BM-derived" myofibroblasts recruited into cancer-induced stroma might also enhance cancer progression. Thus, the elucidation of the recruiting system for BM-derived cells would facilitate better understanding of the biological processes of cancer progression. However, the molecular characters of cancer cells promoting recruitment of BM-derived stromal cells and the mechanism of recruiting stromal cells (especially myofibroblasts) from bone marrow remain largely unknown. Furthermore it is also unknown whether all of cancers always recruit the stromal cells from bone marrow or not.

In order to investigate the effect of different kinds of cancer cell lines on the recruitment of BM-derived vascular endothelial cells (BMD-VE) and myofibroblasts (BMD-MF) in tumor tissue, we used the bone marrow-labeled chimeric immunodeficient mouse and 10 kinds of human cancer cell line. The frequency of BMD-VE (%BMD-VE) and BMD-MF (%BMD-MF) in cancer-induced stroma was assessed and the correlation between the recruitment frequency and tumor-associated parameters [tumor volume (TV), MVD and stromal proportion (%St)] were analyzed. Furthermore in order to assess the effect of tumor growth sites on stromal induction and the recruitment of BMD-VE and -MF, a human pancreatic cancer cell line, Capan-1, was transplanted into 5 different

Abbreviations: BMD-MF, bone marrow-derived myofibroblasts; %BMD-MF, the recruitment frequency of BMD-MF; BMD-VE, bone marrow-derived vascular endothelial cells; %BMD-VE, the recruitment frequency of BMD-VE; GFP, recombination activating gene 1 deficient, enhanced green fluorescence protein transgenic mice; MVD, microvessel density; %St, stromal proportion; RAG-1−/− β-gal, recombination activating gene 1 deficient, Beta-galactosidase transgenic mice; RAG-1−/−; TV, tumor volume.

Grant support: Ministry of Health and Welfare of Japan; Grant number: (15-13), (16-16); Grant support: Ministry of Health and Welfare of Japan.

***Correspondence to:** Pathology Division, National Cancer Center Research Institute East, Chiba, Japan.

Received 13 May 2004; Accepted after revision 29 October 2004
DOI 10.1002/ijc.20969
Published online 23 February 2005 in Wiley InterScience (www.interscience.wiley.com).

sites: subcutaneous tissue, peritoneum, liver, spleen and lung, and then TV, MVD, %St, %BMD-VE and -MF were analyzed.

Material and methods

Animal models

Transgenic mice for Beta-galactosidase (β-gal) (ROSA26, alloantigen: H-2kb), Enhanced green fluorescence protein (GFP mice, alloantigen: H-2kb) and Recombination activating gene-1 deficient mice (RAG-1−/− mice, alloantigen H-2kb) were purchased from The Jackson Laboratory (Bar Harbor, ME). The double-mutant, RAG-1−/− β-gal Tg mice and RAG-1−/− GFP Tg mice were generated in our animal facility, using a previously reported method.[13] Five- to 6-week-old female SCID mice (alloantigen: H-2kd) were purchased from CLEA JAPAN (Tokyo, Japan). All animals were maintained and used in accordance with institutional guidelines under approved protocols.

Bone marrow transplantation (BMT)

About 12 hr after sublethally irradiation (3.5 Gy), the recipient SCID mice received an injection of 1×10^7 BM cells from double mutant mice *via* the tail vein. When mice were sacrificed to harvest the tumor, the success of the BMT was confirmed by flow cytometry analysis of the H-2 phenotype on FACScalibur (Becton Deckinson, Mountain View, CA) as previously described.[13]

Cell culture

The human pancreatic cancer cell line PSN-1 was established and provided by Dr. T. Yoshida (Genetics Division, National Cancer Center, Japan). All other human cancer cell lines were obtained from ATCC (Rockville, MD). Pancreatic cancer cell lines (MIA PaCa-2, PSN-1), breast cancer cell lines (MDA-MB-231, MDA-MB-468), colon cancer cell lines (COLO201, HT-29, SW1116) and hematologic cancer cell lines (HL-60, IM-9) were maintained in a humidified atmosphere of 5% CO_2 in RPMI 1640 medium supplemented with 10% fetal bovine serum. The pancreatic cancer cell line Capan-1 was maintained in RPMI 1640 medium supplemented with 20% fetal bovine serum.

Cell administration and tissue processing

In the subcutaneous implantation model, 10 kinds of human cancer cell line (1×10^7 cells) were subcutaneously injected as a suspension in 200 μl of serum-free medium into the BM-chimera SCID mice at 4 weeks after BMT. Tumors were removed and processed when their diameter reached >10 mm, or at 8 weeks after injection of the cancer cells, whichever occurred first. In the intraperitoneal implantation model, 5×10^6 cells of Capan-1 were injected as a suspension in 200 μl of serum-free medium. Four weeks after injection, mice were sacrificed, and the largest intraperitoneal tumor was examined. In the liver, spleen and lung implantation model, 1×10^6 cells/200 μl of serum-free medium were injected into the spleen (liver and spleen implantation model) under ether anesthesia or *via* the tail vein (lung implantation model). Mice were sacrificed 4 weeks after injection, and each organ was extirpated. All tumor and tissue specimens were fixed in 4% paraformaldehyde-PBS, were washed with sucrose-PBS, embedded in OCT compound (Miles, Inc., Elkhart, IN), quickly frozen in dry ice and stored at −80°C.

X-gal staining

After fixation in 4% paraformaldehyde-PBS for 1 hr on ice, X-gal staining was immediately performed as previously described.[13] After X-gal staining, samples were frozen, sectioned and counterstained with Kernechtrot.

Histological, immunohistochemical, immunofluorescent staining

Prefixed, frozen samples were serially sectioned at 5 μm and processed for H&E staining, immunohistochemistry and immunofluorescent microscopy as previously described.[13] Confocal microscopy was performed in the tumor from RAG-1−/− GFP Tg mice using an LSM5 PASCAL (Carl Zeiss, Jana, Germany). The primary antibodies used here were mouse monoclonal anti-mouse H-2kb (AF6-88.5; PharMingen, San Diego, CA), rat monoclonal anti-mouse CD31 (MEC13.3; PharMingen), mouse monoclonal anti-a smooth muscle actin (α-SMA) (1A4; Sigma Chemical Co., St. Louis, MO), mouse monoclonal anti-multi-cytokeratin (AE1/AE3; Novocastra, UK) and mouse monoclonal anti-human HLA Class I antigen (W6/32; Sigma Chemical Co.). Antibodies for immunofluorescent microscopy were rabbit polyclonal anti-GFP, Alexa Fluor 488 conjugate (Molecular Probes, Eugene, OR) and Alexa Fluor 546 F(ab')2 fragment of goat anti-mouse IgG (Molecular Probes).

Histomorphometric examination

All tumors ($n = 3$, 10 cell lines each) from RAG-1−/− β-gal Tg mice were histomorphometrically analyzed for tumor volume, stromal proportion in the tumor tissue, microvessel density and the proportion of BM-derived cells as previously described.[13,19]

Tumor volume (TV) and stromal proportion (%St)

The diameter of subcutaneous tumors was measured using calipers, and the volume was calculated with the following formula: TV = length (the longest dimension; l) × width (w) × depth × 0.52 (mm^3). The tumor size of other models and the stromal area was measured using the KS 300 system Ver.3.00 (Carl Zeiss). Briefly, tumor length and width were measured by examining the maximum cross sections stained with Hematoxylin and eosin (H&E) (× 5 magnification). At 3 fields, total-tumor area (T) and tumor area (t) occupied by the cancer cells were measured based on those cells staining positive for anti-multi-cytokeratin antibody or anti-human HLA Class I antigen (× 200 magnification). TV and %St was calculated with the following formula: $TV = l \times w^2 \times 0.52$ (mm^3), $\%St = (T - t)/T \times 100$ (%).

Microvessel density (MVD)

Microvessels were counted by scanning serial sections stained with anti-CD31 antibody at 3 fields (× 200 magnification). MVD was expressed as the number of microvessels per field.

Frequency of bone marrow derived vascular endothelial cells (%BMD-VE) and myofibroblasts (%BMD-MF)

After the fields that stained densely with α-SMA were identified, individual antibody-positive cells were counted with serial sections at more than 2 fields (× 400 magnification) by 2 investigators (TS and GI). H-2kb positive cells were counted as BM-derived cells, and then %BMD-VE and %BMD-MF were determined.

Statistical analysis

Statistical analysis was performed using GraphPad Prism Ver.3.03 (GraphPad Software, San Diego, CA). All data were expressed as mean ± standard deviation (SD). Five parameters (TV, %St, MVD, %BMD-VE and %BMD-MF) were analyzed by Spearman's correlation. Correlations with a $p < 0.05$ were considered statistically significant.

Microarray analysis

We used human H133A oligonucleotide probe arrays (Affymetrix, Santa Clara, CA) for analysis of mRNA expression levels corresponding to 22,284 transcripts. The procedures were conducted according to the supplier's protocols, and are thus described briefly. Every 1 mg of total RNA was used to generate a cRNA probe by the T7-transcription. Ten micrograms of fragmented cRNA was hybridized to the microarrays in 200 ml of hybridization cocktail at 45°C for 16 hr in a rotisserie oven set at 60 rpm. The arrays were then washed with nonstringent wash buffer (6 × SSPE) at 25°C, followed by stringent wash buffer [100 mM MES (pH 6.7), 0.1 M NaCl and 0.01% Tween 20] at 50°C, stained with streptavidin phycoerythrin (Molecular Probes), washed again

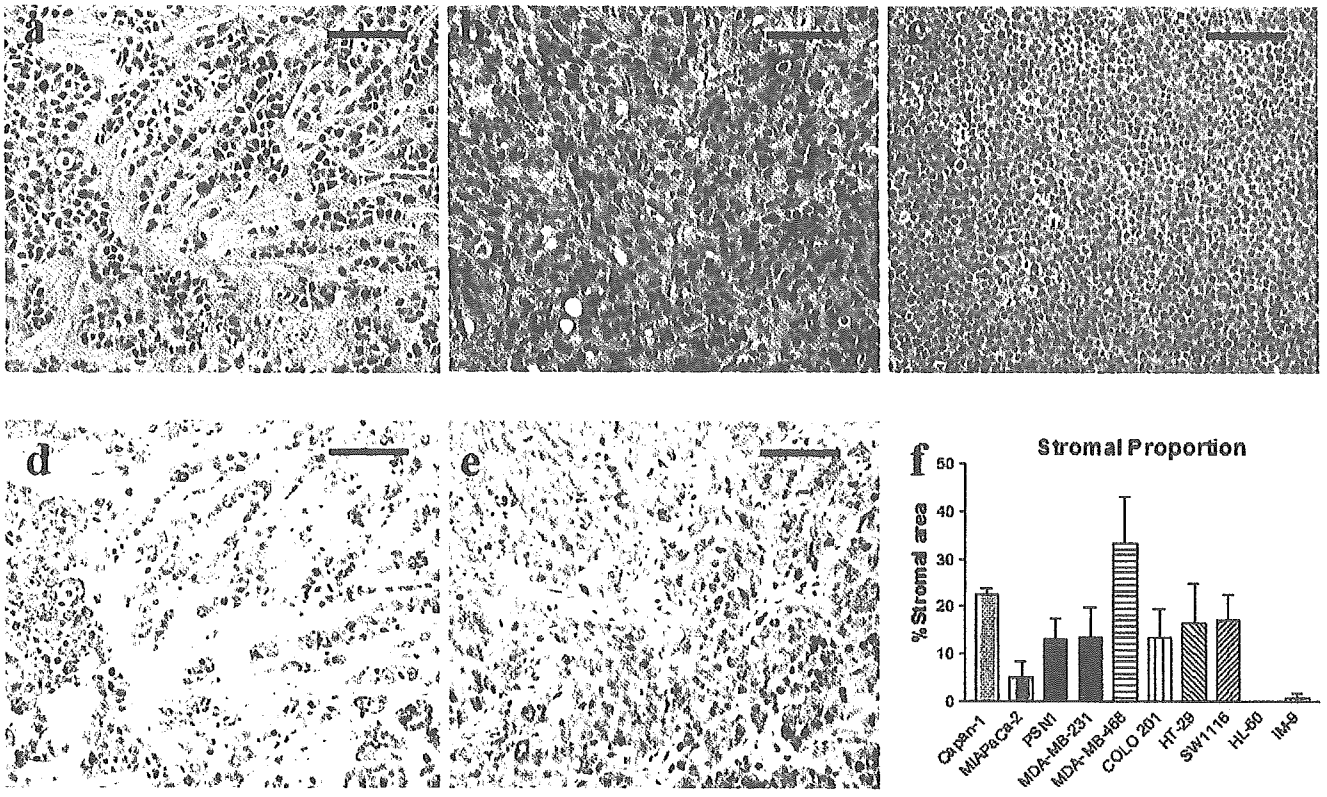

FIGURE 1 – Comparison of cancer-induced stroma in 3 types of cancer cell line. Cancer cells were implanted into the subctaneous tissue of immunodeficient BM-chimera mice and induced various grades of stroma. The difference in the stromal proportion was demonstrated by microscopic appearance with H&E staining (*a–c*) and immunohistochemical staining for multi-cytokeratin (*d,e*). MDA-MB-468 induced the highest grade of stroma (*a,d*). HT29 induced middle grade (*b,e*) but HL-60 failed to induce any stroma (*c*). The result of %St calculated by imaging analysis is summarized (*f*). The data shown represent means ± SD. Bar length: 200 μm.

TABLE I – TUMOR-ASSOCIATED PARAMETERS AND THE FREQUENCY OF BMD-VE AND BMD-MF IN SUBCTANEOUS TUMORS OF VARIOUS CANCER CELL LINES[1]

Cell lines	TV (mm^3)	MVD	%St (%)	%BMD-VE (%)	%BMD-MF (%)
Capan-1	109.3 ± 62.8	55.6 ± 17.7	22.7 ± 1.2	21.6 ± 9.1	29.6 ± 4.0
MIAPaCa-2	80.3 ± 24.2	35.3 ± 14.0	4.9 ± 3.4	6.0 ± 6.0	0.0 ± 0.0
PSN1	83.8 ± 75.5	49.0 ± 8.1	13.2 ± 4.1	5.9 ± 7.4	0.0 ± 0.0
MDA-MB-231	167.9 ± 49.0	49.1 ± 3.9	16.6 ± 3.8	8.8 ± 3.2	20.6 ± 4.8
MDA-MB-468	109.6 ± 57.9	19.9 ± 2.6	31.0 ± 9.0	10.6 ± 13.2	14.0 ± 2.5
COLO 201	186.4 ± 35.0	24.6 ± 0.8	13.5 ± 6.0	7.2 ± 5.6	10.3 ± 12.7
HT-29	512.1 ± 176.4	32.2 ± 12.3	16.4 ± 8.5	5.8 ± 2.2	3.9 ± 1.7
SW1116	200.7 ± 83.8	24.8 ± 7.4	17.2 ± 5.3	8.5 ± 3.9	8.5 ± 6.4
HL-60	392.2 ± 232.3	10.4 ± 3.4	0.0 ± 0.0	0.0 ± 0.0	0.0 ± 0.0
IM-9	740.0 ± 160.6	30.3 ± 12.1	0.7 ± 1.2	0.0 ± 0.0	1.3 ± 2.3

[1]Values are expressed as the mean ± SD.

with 6 × SSPE and stained with biotinylated anti-streptavidin IgG, followed by a second staining with streptavidin phycoerythrin and a 3rd wash with 6 × SSPE. The arrays were scanned using the GeneArray scanner (Affymetrix) at 3-micro m resolution, and the scanned image quantitatively analyzed with the computer software Microarray Suite 5.0 (Affymetrix). For normalizing the data to compare mRNA expression levels among samples, we unified 1,000 as an average of AD scores corresponding to signal intensities of all probe sets in each sample. For statistical analysis to select genes, Microsoft Excel was used.

Results

Desmoplastic reaction in the animal model

H-2 phenotyping of BM cells from the recipient mice demonstrated that BM cells were successfully reconstituted by donor-derived marrows at high levels after BMT, as observed in the previous study.[13] Ten human cancer cell lines (3 pancreas cancers, 2 breast cancers, 3 colon cancers and 2 hematologic cancers) that had been established from different origins were subcutaneously injected into the back of BM chimera mice. They grew and formed various sizes of tumor and demonstrated histological variety (Fig. 1*a–c*). Other human breast cancer cell lines, Hs578T, BT549 and SK-BR-3, were subcutaneously injected; however, they did not show tumorigenicity. When only medium was injected, there was no scar formation and stromal induction was not observed (data not shown). A human breast cancer cell line, MDA-MB-468 induced the most abundant stromal reaction with characteristic desmoplastic features similar to those usually observed in human cancer tissue. A human colon cancer cell line, HT-29 showed a moderate stromal reaction with many spindle-shaped fibroblasts in the tumor. On the other hand, a human promyelocytic leukemia cell line, HL-60 possessed little stromal reaction despite its marked growth. Tumor cells were distinguishable from stromal component more

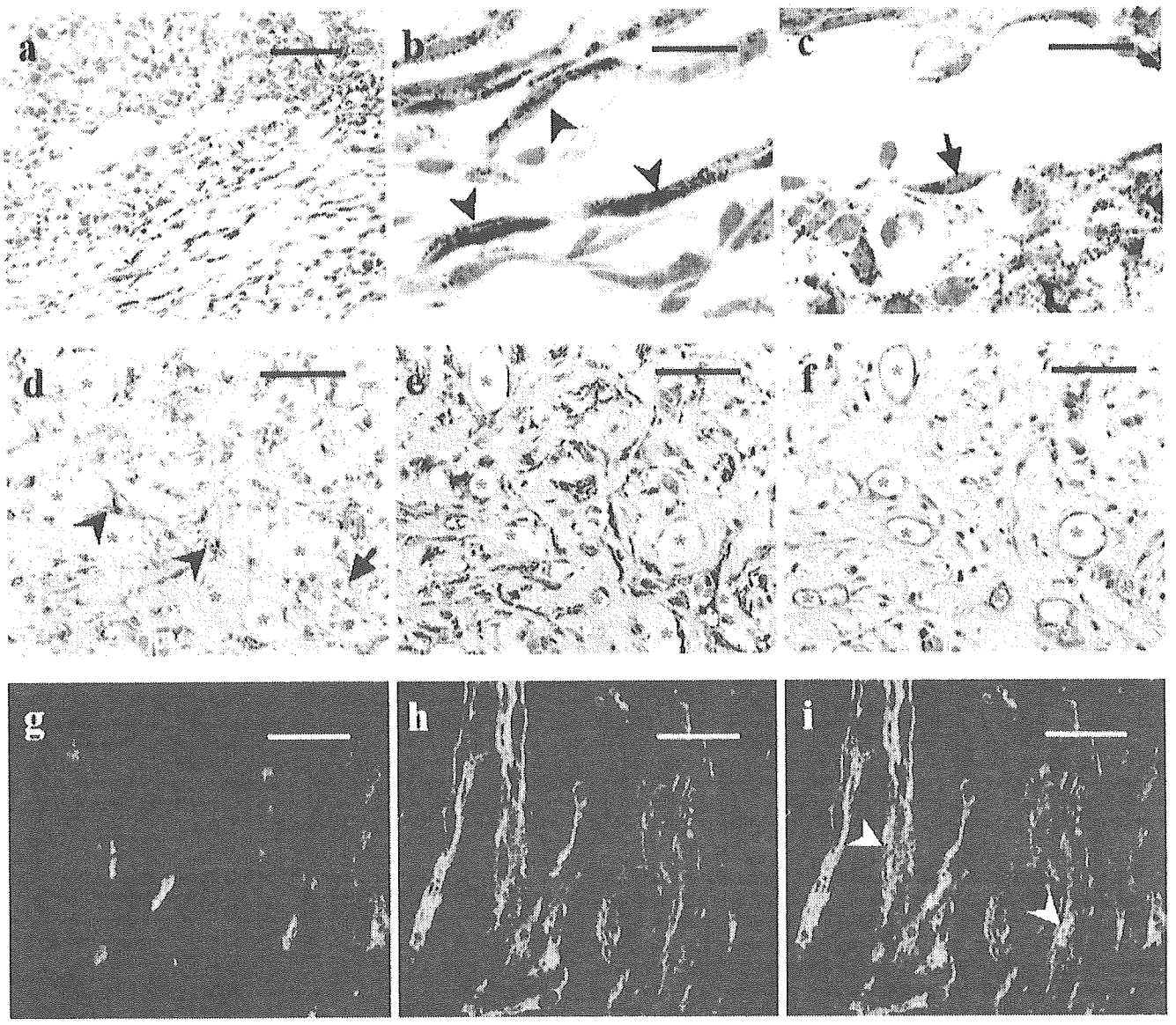

FIGURE 2 – Detection and evaluation of BM-derived stromal cells. BM-derived β-gal expressing cells were detected by X-gal staining as blue-stained cells (*a–c*). The microscopic appearance of MDA-MB-231 tumors showed that blue-stained cells around cancer cells were not only inflammatory cells but also fibroblasts (*b*: arrowheads) and vascular endothelial cells (*c*: arrow). BM-derived stromal cells were also confirmed by anti-H-2kb (*d*), α-SMA (*e*) and CD31 (*f*) with serial sections. Asterisks indicate blood vessels. Arrowheads and arrow indicated BM-derived myofibroblasts and endothelial cells, respectively (*d*). Confocal microscopy identified the GFP (green) positive BM-derived cells (*g*) in the MDA-MB-468 tumor formed in the back of BM-chimera mice. Some of the fibroblasts in the cancer-induced stroma expressed α-SMA (red) (*h*). The merged image shows both α-SMA and GFP positive fibroblasts (BM-derived myofibroblasts) (*i*: arrowheads). Bar length: 200 μm (*a*); 20 μm (*b,c,g–i*); 100 μm (*d–f*).

clearly when the sections were stained with anti-cytokeratin antibody (Fig. 1*d,e*) or anti-human HLA Class I antigen antibody. With the stained sections, imaging analysis was performed using the KS300 system to ascertain %St in the tumor tissue. All data are summarized in Figure 1*f* and Table I. %St of MDA-MB-468 was 31.0±9.0% and the highest value in 10 kinds of cancer cells. %St of HT29 was 16.4±8.5%, and HL-60 was the lowest at 0%.

Detection and evaluation of BM-derived stromal cells

We analyzed β-gal enzyme activity in the extirpated subcutaneous tumor with X-gal whole-mount staining, in order to detect the BM-derived cells. Blue-stained areas were seen in parts of the tumor tissue. The microscopic appearance of MDA-MB-231 tumor showed the β-gal expressing cells as stained blue (Fig. 2*a–c*). The histopathological observation indicated that these were not only inflammatory cells but also fibroblasts (Fig. 2*b*) and vascular endothelial cells (Fig. 2*c*). Further investigations were performed by immunohistochemical staining with anti-mouse H-2kb antibodies, because it was easier than X-gal staining for the detection of BM-derived cells.

Immunohistochemistry with anti-H-2kb antibodies was performed in serial sectioned tumors. In Capan-1 tumors, many H-2kb positive cells were present in the peritumoral and intratumoral area, as previously reported.[13] Furthermore, H-2kb positive cells were also found in the tumors arising from all other cancer cell lines. MDA-MB-468 tumors showed many H-2kb positive cells that contained some spindle-shaped fibroblasts and vascular endothelial cells besides inflammatory cells (Fig. 2*d*). The expression of a-SMA or CD31 as the marker of myofibroblasts or endothelial cells was confirmed by immunohistochemistry using serial sections (Fig. 2*e,f*).

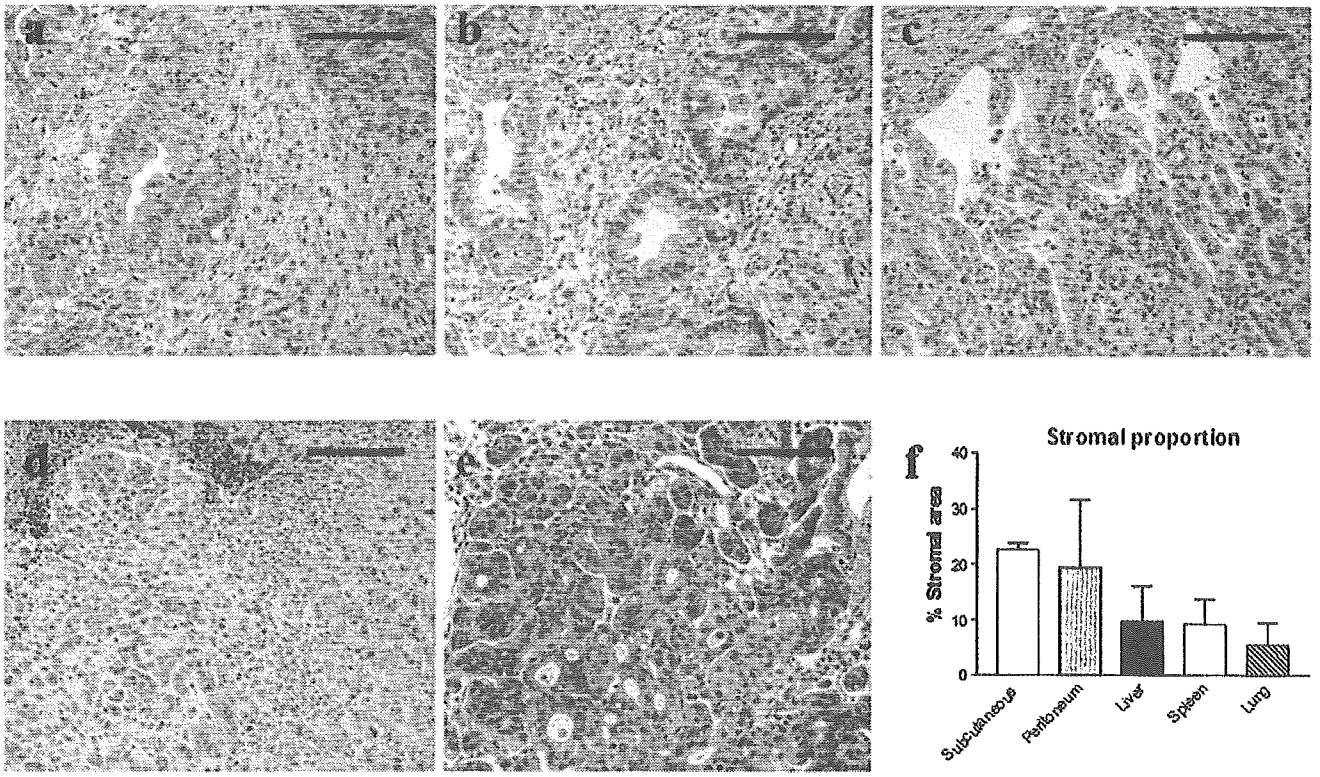

FIGURE 3 – Effect of growth sites on cancer-induced stroma. H&E stained Capan-1 tumors that were implanted in 5 different sites of immunodeficient BM-chimera mice showed histological differences. In the subcutaneous tissue (*a*) and peritoneum (*b*), Capan-1 formed mucous glands with many spindle-shaped fibroblasts. In the liver (*c*), necrosis was frequently observed. In the spleen (*d*), Capan-1 formed poorly differentiated tumors. In the lung (*e*), Capan-1 induced little reactive stroma. After immunohistochemical staining with anti-multi cytokeratin antibody, %St was calculated with imaging analysis. Compared to Capan-1 tumors in the lung, the stromal proportion of Capan-1 tumors in the subctaneous tissue and peritoneum increased 4-fold, and Capan-1 tumors in the liver and spleen increased 2-fold (*f*). Bar length: 200 μm

In order to more precisely confirm the participation of BM-derived stromal cells in tumor tissue, we established another double-mutant mouse (Rag-1−/− GFP Tg). The BM-chimera SCID mouse with BM from this double-mutant mouse is also good for studying the pathogenesis of cancer-induced stroma. Confocal microscopy demonstrated that a part of α-SMA or CD31 positive cells was also stained with anti-GFP antibodies in the MDA-MB-468 tumor tissue sections 8 weeks after subcutaneous injection into the back of BM-chimera mice. Fibroblasts in the cancer-induced stroma displayed 3 different phenotypic expressions: 1) α-SMA+, GFP- fibroblast (α-SMA shows as red), local myofibroblast; 2) α-SMA−, GFP+ fibroblast (GFP shows as green), BM-derived fibroblast and 3) α-SMA+, GFP+ fibroblast (cytoplasm stained red/nuclei stained green), BM-derived myofibroblast (Fig. 3*g–i*).

TABLE II – CORRELATIONS BETWEEN TUMOR-ASSOCIATED FACTORS AND THE FREQUENCY OF BMD-VE AND BMD-MF IN SUBCTANEOUS TUMORS

Variable	Spearman *r*	*p* value (two-tailed)
TV & MVD	−0.4667	0.1786
TV & %St	−0.2606	0.4697
TV & %BMD-VE	−0.5410	0.1139
TV & %BMD-MF	−0.0552	0.8916
MVD & %St	0.2121	0.5603
MVD & %BMD-VE	0.3343	0.3487
MVD & %BMD-MF	0.2638	0.4483
%St & %BMD-VE	0.8875	0.0011
%St & %BMD-MF	0.8283	0.0047
%BMD-VE & %BMD-MF	0.8308	0.0047

Relationship between %stromal area and frequency of bone marrow-derived cells

In order to elucidate whether the participation of BMD-VE and -MF in the cancer-induced stroma depended on tumor phenotype, the frequency of BM-derived cells (%BMD-VE and %BMD-MF) and tumor-associated parameters (TV, MVD and %St) were calculated (Table I). In most of the cancer cell lines, BM-derived cells participated in a part of the cancer-induced stroma as either vessel endothelium or myofibroblast. The highest average frequency of BMD-VE and BMD-MF was 21.6±9.1% and 29.6±4.0% in Capan-1-induced stroma.

We then analyzed the correlation among these parameters (Table II). Both %BMD-VE and %BMD-MF significantly correlated with %St ($p = 0.0011$, $p = 0.0047$, respectively). %BMD-VE strongly correlated with %BMD-MF ($p = 0.0047$) but did not correlate with MVD ($p = 0.3487$). There was no correlation between TV and MVD and %St.

Effect of growth sites on cancer-induced stroma

In order to demonstrate whether the BM-derived stromal cells recruitment was associated with specific sites, Capan-1 was implanted in the subcutaneous tissue, peritoneum, liver, spleen and lung. Capan-1 tumors that grew up in the various sites showed different morphologies with varying amounts of stroma. Capan-1 formed glands with mucus production in the subcutaneous tissue, peritoneum, liver and lung, but they formed solid nests without mucin-producing glands in the spleen. Concerning stromal reactions, Capan-1 induced desmoplastic stroma where spindle-shaped fibroblasts were seen, arranged in a haphazard fashion in the subcutaneous and intraperitoneal tumors. In contrast, Capan-1 induced only

TABLE III – TUMOR-ASSOCIATED PARAMETERS AND THE FREQUENCY OF BMD-VE AND BMD-MF IN CAPAN-1 TUMORS GROWN IN THE VARIOUS SITES[1]

Implantation site	TV (mm^3)	MVD	%St (%)	%BMD-VE (%)	%BMD-MF (%)
Subcutaneous tissue	109.3 ± 62.8	55.6 ± 17.7	22.7 ± 1.2	21.6 ± 9.1	29.6 ± 4.0
Peritoneum	74.9 ± 48.0	25.7 ± 9.5	19.5 ± 12.1	16.5 ± 4.6	24.5 ± 12.5
Liver	30.9 ± 14.9	8.7 ± 3.1	9.7 ± 6.4	0.0 ± 0.0	0.0 ± 0.0
Spleen	8.5 ± 5.2	12.4 ± 5.6	9.1 ± 4.6	0.0 ± 0.0	0.0 ± 0.0
Lung	0.5 ± 0.3	13.3 ± 5.0	5.4 ± 3.9	0.0 ± 0.0	0.0 ± 0.0

[1]Values are expressed as the mean ± SD.

minor amounts of stroma at the liver, spleen and lung. Necrosis was frequently observed in the larger liver tumors. Only small numbers of reactive fibroblasts were observed in the peritumoral area of liver and spleen. Small tumors showed no reactive stroma in the lung.

The frequency of BM-derived cells (%BMD-VE and %BMD-MF) and 3 tumor-associated parameters (TV, MVD and %St) were calculated in order to disclose the growth site-associated effect on recruitment of BMD-VE and -MF (Table III). %St of subcutaneous tumors was 22.7±1.2%, and of intraperitoneal tumors was 19.5±12.1%. On the other hand, the value for the %St of liver, splenic and lung tumors were much lower (9.7±6.4%, 9.1±4.6% and 5.4±3.9%, respectively). In the subcutaneous tissue and peritoneum, BMD-VE and -MF were recruited to Capan-1 tumors in a stromal proportion-dependent manner, whereas no BMD-VE or -MF could be identified in Capan-1 induced stroma in the liver, spleen and lung.

Comparison between the expression profiles of cancer cell lines inducing an abundant stromal reaction and little stromal reaction

To identify the genes whose products are involved in the formation of reactive stroma and recruitment of BMD-VE and -MF, 10 human cancer cell lines were separated into 3 groups: a group that induces an abundant stromal reaction (Capan-1 and MDA-MB-468), a group that induces a moderate stromal reaction (PSN-1, MDA-MB-231, COLO201, HT-29 and SW1116) and a group that induces little stromal reaction (MIA PaCa-2 and HL-60, IM-9). Genome-wide screening for genes with different expression patterns in the 3 groups was performed using a microarray containing 22,284 probes. We first selected genes whose average expression in the moderate-stromal-reaction group was greater than 2 fold up- or down-regulated compared to the little-stromal-reaction group. From among these genes, we then selected the genes that were expressed more than 2-fold more or 2-fold less in the abundant-stromal-reaction group than in the moderate-stromal-reaction group (Table IV). Although they included genes that encode membrane receptors, adhesion/polarization molecules and extracellular matrix components and their receptors, and transcription factors, they did not contain the well-known genes whose products are directly involved in stromal cell recruitment, differentiation and proliferation.

Discussion

It is well recognized that endothelial cells are required for vascularization during tissue remodeling,[12,20] and stromal fibroblasts or myofibroblasts are ubiquitous cells and regulate the proliferation and differentiation of both normal and abnormal epithelial cells.[14,16–18,21–24] We recently demonstrated that a significant proportion of myofibroblasts was recruited from the BM and had proliferative activity in the subcutaneously transplanted tumors of a human pancreatic cancer cell line, Capan-1.[13] In our study, we clearly demonstrated that 7 other human cancer cell lines also recruited BMD-VE and/or -MF into the cancer stroma in the subcutaneous tissue and induced neovascularization and myofibroblast proliferation to a greater or less extent. Furthermore, there was a positive correlation between the proportion of stroma (%St) and the frequency of BMD-VE and -MF (%BMD-VE and -MF) in the subcutaneous tumors. These results indicated that the recruitment of BMD-VE and -MF is a general phenomenon during cancer-induced stroma formation.

The origin of BMD-MF and the molecules involved in their directed migration remain unclear. The results obtained in our study revealed a strong correlation between the frequency of BMD-VE and BMD-MF and the following 2 possibilities were considered to explain this phenomenon. The first is that common progenitor cells differentiate into both BMD-VE and BMD-MF in the local cancer tissue. Earlier studies have reported that adult-blood-derived CD34+VEGFR-2+ angioblasts differentiated into endothelial cells,[11,25,26] and recent cumulative findings have suggested that peripheral-blood-derived mature CD14+ monocytes are also capable of transdifferentiating into endothelial lineage cells under angiogenic conditions.[27–29] On the other hand, it has been reported that CD14+ enriched peripheral mononuclear cells give rise to fibrocytes[30–32] and that these fibrocytes differentiate into myofibroblasts *in vitro*[30] and *in vivo*.[33] The above findings suggest that CD14+ mononuclear cells may be the common progenitor of BMD-VE and -MF. The second possibility is that both BMD-VE and BMD-MF progenitor cells are recruited into cancer tissue by a common molecular mechanism. Endothelial progenitor cells express CXCR4 and migrate in response to stromal cell derived factor-α (SDF-1),[25] and they promote neovascularization for ischemic muscle,[34] whereas BM-derived fibroblasts obtained from lung fibrosis expressed the chemokine receptors CXCR4 and CCR7 and responded chemotactically to their cognate ligands, SDF-1 and secondary lymphoid chemokine (CXCL21), respectively.[35] Thus SDF-1 may be a key regulator of the recruitment of vascular endothelial and myofibroblast progenitor cells from BM during stroma formation.

Microarray analysis identified 29 genes differentially expressed in the group that induced an abundant stromal reaction. Among them, upregulated genes, such as *epidermal growth factor receptor, transmembrane 4 superfamily member 13, tropomyosin 1, carcinoembryonic antigen-related cell adhesion molecule 6, junction plakoglobin, desmoplakin, mucin 1 and integrin alpha V*, seem to reflect the epithelial phenotype and include important genes for cell-cell and -substratum adhesion. But these genes could be picked up even when microarray analysis was performed without hematologic cancer cell lines (date not shown). Further analysis should be directed at addressing the exact role of these genes with regard to BMD-VE and -MF recruitment by gene overexpression or silencing methods. We were unable to find the well-known genes whose products are directly involved in stromal cell recruitment (chemokines), differentiation (cytokines) or proliferation (growth factors). Because the interactions between cancer cells and host stromal cells are greatly important in cancer-induced stromal reaction, identification of key molecules might be difficult by only *in vitro* experiment. An analysis of the tissue specimen using microdissection technique would be required to identify the molecules that are directly involved in stromal reaction and BM-derived stromal cells' recruitment.

A human pancreatic cancer cell line, Capan-1, which formed subcutaneous and peritoneal tumors with a relatively high proportion of stroma, failed to induce active stroma when implanted into the liver, spleen or lung, and a significant proportion of BMD-VE and -MF were recruited into the subcutaneous and peritoneal tumors but not into the spleen or lung. Furthermore, Capan-1

TABLE IV – cDNA MICROARRAY SEARCH FOR GENES THAT ARE DIFFERENTIALLY EXPRESSED IN CELL LINES THAT INDUCE AN ABUNDANT STROMAL REACTION

Accession number	Gene name	Ratio 1[1]	Ratio 2[2]
Genes upregulated in cell lines inducing abundant stromal reaction			
Extracellular matrix components and receptors			
NM002456	mucin 1	17.3	3.8
NM002210	integrin alpha V	8.0	2.7
Adhesion/polarization			
NM000366	tropomyosin 1	27.2	6.5
NM002483	carcinoembryonic antigen-related cell adhesion molecule 6	24.7	7.4
NM002230	junction plakoglobin	21.2	8.6
NM004415	desmoplakin	14.8	6.8
Membrane receptors			
NM014399	transmembrane 4 superfamily member 13	100<	37.3
NM005228	epidermal growth factor receptor	20.5	3.7
Transcription factors			
NM003489	nuclear receptor interacting protein 1	100<	100<
NM002051	GATA binding protein 3	43.1	8.2
NM015925	liver-specific bHLH-Zip transcription factor	34.2	15.4
NM006368	cAMP responsive element binding protein 3	12.0	4.5
NM005596	nuclear factor I/B	8.0	2.9
Signal transduction			
NM002353	tumor-associated calcium signal transducer 2	100<	100<
NM004815	PTPL1-associated RhoGAP 1	26.1	12.5
NM005766	FERM, RhoGEF and pleckstrin domain protein 1	13.3	5.4
RNA and protein synthesis			
NM002952	ribosomal protein S2	7.9	3.1
Proliferation/apoptosis			
NM004585	retinoic acid receptor responder 3	20.9	9.2
NM006142	stratifin	9.9	3.4
NM020749	mitochondrial tumor suppressor 1	9.8	2.1
NM004394	death-associated protein	5.4	2.6
Others			
NM002844	protein tyrosine phosphatase, receptor type, K	100<	100<
NM020169	latexin	26.1	12.5
NM002970	spermidine N1 acetyltransferase	13.3	5.4
NM002959	sortilin 1	7.9	3.9
Genes downregulated in cell lines inducing abundant stromal reaction			
Signal transduction			
NM004811	leupaxin	0.1	0.4
RNA and protein synthesis			
NM001970	Eukaryotic translation initiation factor 5A	0.1	0.3
Others			
NM004955	Solute carrier family 29	0.2	0.5
NM013300	Protein predicted by clone 23733	0.2	0.5

[1]Ratio 1: A group that induces an abundant stromal reaction/moderate stromal reaction.–[2]Ratio 2: A group that induces a moderate stromal reaction/ little stromal reaction.

tumors in the liver undergo massive necrosis without recruitment of BMD-VE and -MF. These results suggest the microenvironment of the liver might be suitable for tumorigenesis by Capan-1 but not for inducing stromal component and maintaining themselves. BMD-VE and -MF were also recruited into pathological neovascularization and fibrosis under the condition of inflammation and regeneration without cancer cells.[29,35–37] These results may indicate that the mechanism of the stromal reaction and recruitment of BMD-VE and -MF does not depend on the biological character of the cancer cells themselves but on the microenvironment created by the cancer-stroma interaction.

Tumor angiogenesis is essential for tumor growth, and intratumoral microvessel density has been found to correlate with tumor progression. We did not find any correlation between MVD and %BMD-VE in our study. Although BMD-VE was incorporated into some newly developed microvessels, the %BMD-VE varied with the characteristics of the cancer. This seems to indicate that the recruitment of BMD-VE into microvessels required for the neovascularization might be influenced by cancer microenvironment.

Even though MVD is a useful prognostic factor in some cancer patients, previous studies found that intratumoral MVD in breast carcinoma does not correlate with tumor cell proliferation,[38] and their findings are consistent with our results showing that TV does not correlate with MVD. Therefore, MVD and tumor cell proliferation may be regulated by separate mechanisms.

Surgically resected specimens of certain kinds of cancers, *i.e.*, malignant lymphoma and small cell carcinoma, have been found not to contain active stroma. Therefore, our results showing that TV did not correlate with %St are reasonable and may be explained by the fact that the HL-60 and IM-9 used in our study do not need stromal cell components for the development and maintenance of cancer tissue. MIAPaCa-2 and PSN-1 had the lowest TV and these tumors had lower %St. This finding seems to corroborate the idea that tumor growth would not be suppressed by cancer-induced stroma. The fact that when Capan-1 was implanted at different sites, TV increased with %St supports this view. Alternatively, stromal components are required for certain kinds of cancer cells to develop cancer tissue.

Because BMD-VE and -MF are generally engrafted into a stroma-inductive type of cancer tissue, endothelial and myofibroblast progenitors may be used as a vehicle for biological agent and gene therapy.[39,40] Moreover, the cancer tissue microenvironment requires more vascular endothelium and myofibroblasts to main-

tain "tissue homeostasis" than the normal tissue microenvironment. Just as drugs that target the tumor context and inhibit neovascularization are already recognized as effective means of cancer therapy,[41,42] inhibition of myofibroblasts recruitment into the cancer tissue may also be effective as a new therapy for the stroma-inductive type of cancer.

Acknowledgements

We thank C. Okumura and Y. Okuhara for their expert technical assistance, and M. Suzaki for secretarial assistance. T. S., K. K. and S. M. are Awardees of Research Resident Fellowships from the Foundation for Promotion of Cancer Research in Japan.

References

1. Liotta LA, Kohn EC. The microenvironment of the tumour-host interface. Nature 2001;411:375–9.
2. Matrisian LM, Cunha GR, Mohla S. Epithelial-stromal interactions and tumor progression: meeting summary and future directions. Cancer Res 2001;61:3844–6.
3. Hanahan D, Weinberg RA. The hallmarks of cancer. Cell 2000;100:57–70.
4. Fontanini G, Bigini D, Vignati S, Basolo F, Mussi A, Lucchi M, Chine S, Angeletti CA, Harris AL, Bevilacqua G. Microvessel count predicts metastatic disease and survival in non-small cell lung cancer. J Pathol 1995;177:57–63.
5. Hasan J, Byers R, Jayson GC. Intra-tumoural microvessel density in human solid tumours. Br J Cancer 2002;86:1566–77.
6. Nishimura R, Hasebe T, Tsubono Y, Ono M, Sugitoh M, Arai T, Mukai K. The fibrotic focus in advanced colorectal carcinoma: a hitherto unrecognized histological predictor for liver metastasis. Virchows Arch 1998;433:517–22.
7. Weidner N, Semple JP, Welch WR, Folkman J. Tumor angiogenesis and metastasis: correlation in invasive breast carcinoma. N Engl J Med 1991;324:1–8.
8. Hasebe T, Mukai K, Tsuda H, Ochiai A. New prognostic histological parameter of invasive ductal carcinoma of the breast: clinicopathological significance of fibrotic focus. Pathol Int 2000;50:263–72.
9. Henry N, van Lamsweerde AL, Vaes G. Collagen degradation by metastatic variants of Lewis lung carcinoma: cooperation between tumor cells and macrophages. Cancer Res 1983;43:5321–7.
10. Coussens LM, Tinkle CL, Hanahan D, Werb Z. MMP-9 supplied by bone marrow-derived cells contributes to skin carcinogenesis. Cell 2000;103:481–90.
11. Asahara T, Masuda H, Takahashi T, Kalka C, Pastore C, Silver M, Kearne M, Magner M, Isner JM. Bone marrow origin of endothelial progenitor cells responsible for postnatal vasculogenesis in physiological and pathological neovascularization. Circ Res 1999;85:221–8.
12. Carmeliet P, Jain RK. Angiogenesis in cancer and other diseases. Nature 2000;407:249–57.
13. Ishii G, Sangai T, Oda T, Aoyagi Y, Hasebe T, Kanomata N, Endoh Y, Okumura C, Okuhara Y, Magae J, Emura M, Ochiya T, et al. Bone-marrow-derived myofibroblasts contribute to the cancer-induced stromal reaction. Biochem Biophys Res Commun 2003;309:232–40.
14. Ronnov-Jessen L, Petersen OW, Bissell MJ. Cellular changes involved in conversion of normal to malignant breast: importance of the stromal reaction. Physiol Rev 1996;76:69–125.
15. Iozzo RV. Tumor stroma as a regulator of neoplastic behavior: agonistic and antagonistic elements embedded in the same connective tissue. Lab Invest 1995;73:157–60.
16. Noel A, Foidart JM. The role of stroma in breast carcinoma growth in vivo. J Mammary Gland Biol Neoplasia 1998;3:215–25.
17. Gregoire M, Lieubeau B. The role of fibroblasts in tumor behavior. Cancer Metastasis Rev 1995;14:339–50.
18. Martin M, Pujuguet P, Martin F. Role of stromal myofibroblasts infiltrating colon cancer in tumor invasion. Pathol Res Pract 1996;192:712–7.
19. Jitsuiki Y, Hasebe T, Tsuda H, Imoto S, Tsubono Y, Sasaki S, Mukai K. Optimizing microvessel counts according to tumor zone in invasive ductal carcinoma of the breast. Mod Pathol 1999;12:492–8.
20. Kocher AA, Schuster MD, Szabolcs MJ, Takuma S, Burkhoff D, Wang J, Homma S, Edwards NM, Itescu S. Neovascularization of ischemic myocardium by human bone-marrow-derived angioblasts prevents cardiomyocyte apoptosis, reduces remodeling and improves cardiac function. Nat Med 2001;7:430–6.
21. van Roozendaal KE, Klijn JG, van Ooijen B, Claassen C, Eggermont AM, Henzen-Logmans SC, Foekens JA. Differential regulation of breast tumor cell proliferation by stromal fibroblasts of various breast tissue sources. Int J Cancer 1996;65:120–5.
22. Bostrom H, Willetts K, Pekny M, Leveen P, Lindahl P, Hedstrand H, Pekna M, Hellstrom M, Gebre-Medhin S, Schalling M, Nilsson M, Kurland S, et al. PDGF-A signaling is a critical event in lung alveolar myofibroblast development and alveogenesis. Cell 1996;85:863–73.
23. Karlsson L, Lindahl P, Heath JK, Betsholtz C. Abnormal gastrointestinal development in PDGF-A and PDGFR-(alpha) deficient mice implicates a novel mesenchymal structure with putative instructive properties in villus morphogenesis. Development 2000;127:3457–66.
24. Darcy KM, Zangani D, Shea-Eaton W, Shoemaker SF, Lee PP, Mead LH, Mudipalli A, Megan R, Ip MM. Mammary fibroblasts stimulate growth, alveolar morphogenesis, and functional differentiation of normal rat mammary epithelial cells. In Vitro Cell Dev Biol Anim 2000;36:578–92.
25. Peichev M, Naiyer AJ, Pereira D, Zhu Z, Lane WJ, Williams M, Oz MC, Hicklin DJ, Witte L, Moore MA, Rafii S. Expression of VEGFR-2 and AC133 by circulating human CD34(+) cells identifies a population of functional endothelial precursors. Blood 2000;95:952–8.
26. Shi Q, Rafii S, Wu MH, Wijelath ES, Yu C, Ishida A, Fujita Y, Kothari S, Mohle R, Sauvage LR, Moore MA, Storb RF, et al. Evidence for circulating bone marrow-derived endothelial cells. Blood 1998;92:362–7.
27. Harraz M, Jiao C, Hanlon HD, Hartley RS, Schatteman GC. CD34-blood-derived human endothelial cell progenitors. Stem Cells 2001;19:304–12.
28. Rehman J, Li J, Orschell CM, March KL. Peripheral blood "endothelial progenitor cells" are derived from monocyte/macrophages and secrete angiogenic growth factors. Circulation 2003;107:1164–9.
29. Fujiyama S, Amano K, Uehira K, Yoshida M, Nishiwaki Y, Nozawa Y, Jin D, Takai S, Miyazaki M, Egashira K, Imada T, Iwasaka T, et al. Bone marrow monocyte lineage cells adhere on injured endothelium in a monocyte chemoattractant protein-1-dependent manner and accelerate reendothelialization as endothelial progenitor cells. Circ Res 2003;93:980–9.
30. Abe R, Donnelly SC, Peng T, Bucala R, Metz CN. Peripheral blood fibrocytes: differentiation pathway and migration to wound sites. J Immunol 2001;166:7556–62.
31. Yang L, Scott PG, Giuffre J, Shankowsky HA, Ghahary A, Tredget EE. Peripheral blood fibrocytes from burn patients: identification and quantification of fibrocytes in adherent cells cultured from peripheral blood mononuclear cells. Lab Invest 2002;82:1183–92.
32. Kuwana M, Okazaki Y, Kodama H, Izumi K, Yasuoka H, Ogawa Y, Kawakami Y, Ikeda Y. Human circulating CD14+ monocytes as a source of progenitors that exhibit mesenchymal cell differentiation. J Leukoc Biol 2003;74:833–45.
33. Schmidt M, Sun G, Stacey MA, Mori L, Mattoli S. Identification of circulating fibrocytes as precursors of bronchial myofibroblasts in asthma. J Immunol 2003;171:380–9.
34. Yamaguchi J, Kusano KF, Masuo O, Kawamoto A, Silver M, Murasawa S, Bosch-Marce M, Masuda H, Losordo DW, Isner JM, Asahara T. Stromal cell-derived factor-1 effects on ex vivo expanded endothelial progenitor cell recruitment for ischemic neovascularization. Circulation 2003;107:1322–8.
35. Hashimoto N, Jin H, Liu T, Chensue SW, Phan SH. Bone marrow-derived progenitor cells in pulmonary fibrosis. J Clin Invest 2004;113:243–52.
36. Gao Z, McAlister VC, Williams GM. Repopulation of liver endothelium by bone-marrow-derived cells. Lancet 2001;357:932–3.
37. Direkze NC, Forbes SJ, Brittan M, Hunt T, Jeffery R, Preston SL, Poulsom R, Hodivala-Dilke K, Alison MR, Wright NA. Multiple organ engraftment by bone-marrow-derived myofibroblasts and fibroblasts in bone-marrow-transplanted mice. Stem Cells 2003;21:514–20.
38. Vartanian RK, Weidner N. Correlation of intratumoral endothelial cell proliferation with microvessel density (tumor angiogenesis) and tumor cell proliferation in breast carcinoma. Am J Pathol 1994;144:1188–94.
39. Studeny M, Marini FC, Champlin RE, Zompetta C, Fidler IJ, Andreeff M. Bone marrow-derived mesenchymal stem cells as vehicles for interferon-beta delivery into tumors. Cancer Res 2002;62:3603–8.
40. Ferrari N, Glod J, Lee J, Kobiler D, Fine HA. Bone marrow-derived, endothelial progenitor-like cells as angiogenesis-selective gene-targeting vectors. Gene Ther 2003;10:647–56.
41. Lyden D, Hattori K, Dias S, Costa C, Blaikie P, Butros L, Chadburn A, Heissig B, Marks W, Witte L, Wu Y, Hicklin D, et al. Impaired recruitment of bone-marrow-derived endothelial and hematopoietic precursor cells blocks tumor angiogenesis and growth. Nat Med 2001;7:1194–201.
42. Tonini T, Rossi F, Claudio PP. Molecular basis of angiogenesis and cancer. Oncogene 2003;22:6549–56.

STEM CELLS®
Original Article

In Vivo Characterization of Bone Marrow–Derived Fibroblasts Recruited into Fibrotic Lesions

GENICHIRO ISHII,[a] TAKAFUMI SANGAI,[a] KENJI SUGIYAMA,[b] TAKASHI ITO,[a,c] TAKAHIRO HASEBE,[a] YASUSHI ENDOH,[a] JUNJI MAGAE,[d] ATSUSHI OCHIAI[a,c]

[a]Pathology Division, and [b]Investigative Treatment Division, National Cancer Center Research Institute East, Kashiwa, Chiba, Japan; [c]Laboratory of Cancer Biology, Department of Integrated Biosciences, Graduate School of Frontier Sciences, University of Tokyo, Kashiwa, Chiba, Japan; [d]Department of Biotechnology, Institute of Research and Innovation, Kashiwa, Chiba, Japan

Key Words. Bone marrow–derived fibroblasts • Green fluorescent protein

ABSTRACT

Fibroblasts, which are widely distributed and play a key part in tissue fibrosis, are phenotypically and functionally heterogeneous. Recent studies reported that bone marrow can be a source of tissue fibroblast. In the study reported here, we investigated in vivo characterization of bone marrow–derived fibroblasts recruited into various fibrotic lesions. Mice were engrafted with bone marrow isolated from transgenic mice expressing green fluorescent protein (GFP), and fibrotic lesions were induced by cancer implantation (skin), excisional wounding (skin), and bleomycin administration (lung). A small population of GFP$^+$ fibroblast was found even in nonfibrotic skin (8.7% ± 4.6%) and lung (8.9% ± 2.5%). The proportion of GFP$^+$ fibroblasts was significantly increased after cancer implantation (59.7% ± 16.3%) and excisional wounding (32.2% ± 4.8%), whereas it was not elevated after bleomycin administration (7.1% ± 2.4%). Almost all GFP$^+$ fibroblasts in fibrotic lesions expressed type I collagen, suggesting that bone marrow–derived fibroblasts would contribute to tissue fibrosis. GFP$^+$ fibroblasts expressed CD45, Thy-1, and α-smooth muscle actin at various proportions. Our results suggested that bone marrow–derived fibroblasts expressed several fibroblastic markers in vivo and could be efficiently recruited into fibrotic lesions in response to injurious stimuli; however, the degree of recruitment frequency might depend on the tissue microenvironment. STEM CELLS *2005;23:699–706*

INTRODUCTION

Injury evokes a sequence of events in tissue. Once injury occurs, the host initiates a coordinated repair response. However, if the injury is prolonged, a repeated process of repair and destruction occurs, which subsequently leads to tissue remodeling. During the process, tissue fibroblasts migrate into the injured site and produce collagens and extracellular matrix proteins in response to several extracellular stimuli. Their functions include important roles in growth and differentiation of adjacent epithelia and healing and inflammatory response. Fibroblasts represent the key source of interstitial collagens, but these cells are known to be heterogeneous with respect to a number of phenotypic and functional features [1–6]. This heterogeneity may arise not only from the activation and differentiation processes that take place in the cells but from their different cellular origins.

Stem cells in the adult have traditionally been thought to be restricted in their potential to differentiate and regenerate tissues in which they reside. Recent advances have revealed that after

Correspondence: Atsushi Ochiai, M.D., Ph.D., Pathology Division, National Cancer Center Research Institute East, 6-5-1 Kashiwanoha, Kashiwa-City, Chiba 277-8577, Japan. Telephone: 81-4-7134-6855; Fax: 81-4-7134-6865; e-mail: aochiai@east.ncc.go.jp Received August 9, 2004; accepted for publication January 5, 2005. 1066-5099/2005/$12.00/0 doi: 10.1634/stemcells.2004-0183

transplantation of bone marrow (BM), hematopoietic stem cells or nonhematopoietic mesenchymal stem cells, muscle [7–11], heart [12–14], liver [15–19], vascular cells [20, 21], and other mesenchymal cells [22–24] of donor origin have been detected. Investigators revealed that BM-derived cells can be progenitors for tissue fibroblasts that are recruited through the circulation to populate peripheral organs [25–29]. During renal fibrosis, a small number of fibroblasts were BM origin using BM chimera and transgenic reporter mice [25]. We previously reported that cancer-induced stroma generated by the human pancreatic cancer cell line consist of BM-derived fibroblasts and that BM-derived fibroblasts become a major component of cancer-induced stromal cells in the later stage of tumor development [26]. Furthermore, BM-derived fibroblasts were engrafted into multiple organs, and it was found that these cells are recruited into injured tissue [27, 28]. However, the phenotype and functional roles of BM-derived fibroblasts have not been fully understood.

In the study reported here, we investigated the possible relationship between BM-derived fibroblasts and various fibroblast phenotypes. Cancer implantation (skin), excisional wounding (skin), and bleomycin administration (lung) were used to assess whether fibroblast engraftment was modulated by tissue damage and to analyze the phenotypes of BM-derived fibroblasts. Using BM chimera mice expressing enhanced green fluorescent protein (GFP) only in BM-derived cells, we found that excisional wounding is a stimulus for the recruitment of BM-derived fibroblasts within the skin but not in the lung. Furthermore, we found that BM-derived fibroblasts expressed type I collagen, CD45, Thy-1, and α-smooth muscle actin (α-SMA).

Materials and Methods

Animals

For cancer implantation, we generated GFP transgenic (GFP Tg) and recombination activating gene 1 knockout (RAG-$1^{-/-}$) double-mutant mice. GFP Tg on C57/BL6 background and RAG-$1^{-/-}$ mice on B6 background [30] were purchased from Jackson ImmunoResearch Laboratories (West Grove, PA, http://www.jacksonimmuno.com). Briefly, the GFP Tg mice were mated with RAG-$1^{-/-}$ mice to generate F1 offspring that were heterogenous for both genes. The F2 offspring of the F1 interbreeding were screened by Western blot analysis for absence of serum immunoglobulin M (IgM) [19]. Mice identified as $GFP^{+/-}$ were screened for fluorescence of skin keratinocytes. RAG-$1^{-/-}$ GFP Tg mice that were identified were further intercrossed, and the F3 offspring were screened based on serum IgM level and GFP fluorescence. GFP Tg and RAG-$1^{-/-}$ mice were further bred. For BM transplantation (BMT), female severe combined immunodeficient (SCID) mice (C.B17 background) and C57/BL6 mice, 6 weeks of age, were purchased from Clea Japan, Inc. (Tokyo, http://www.clea-japan.co.jp) and maintained in our animal facility. All animals were maintained under specific pathogen-free and air temperature–controlled conditions throughout this study, in accordance with the institutional guidelines. Written approval of all animal experiments (K03-011) was obtained from the local Animal Experiments Committee of the National Cancer Center Research Institute.

Cell Preparation and BMT

A 21-gauge needle on a 5-ml syringe was used to flush BM from the femurs of GFP Tg RAG-$1^{-/-}$ mice or GFP Tg mice with RPMI-1640 medium. A single-cell suspension was prepared by repeated gentle aspirations of the marrow plug with the same syringe, and large tissue pieces were removed from the suspension by filtering them through a nylon filter. After 3.5-Gy whole-body irradiation of SCID mice or 9-Gy whole-body irradiation of B6 mice with a 50,000 Ci ^{60}Co source in the irradiation room, 1×10^7 donor marrow cells were injected via the tail vein.

Cancer Implantation, Excisional Wounding, and Bleomycin Administration

For creating fibrotic lesions induced by cancer implantation, we transplanted marrow cells from GFP Tg RAG-$1^{-/-}$ mice into irradiated (3.5 Gy) SCID mice. At 4 weeks after BMT, we subcutaneously inoculated SCID recipients with a transplantable human large-cell neuroendocrine carcinoma of the lung (613LCNEC), which was established in our laboratory and propagated in SCID mice for more than 10 passages. Four weeks later, tumors that had developed were resected and examined histologically (Fig. 1).

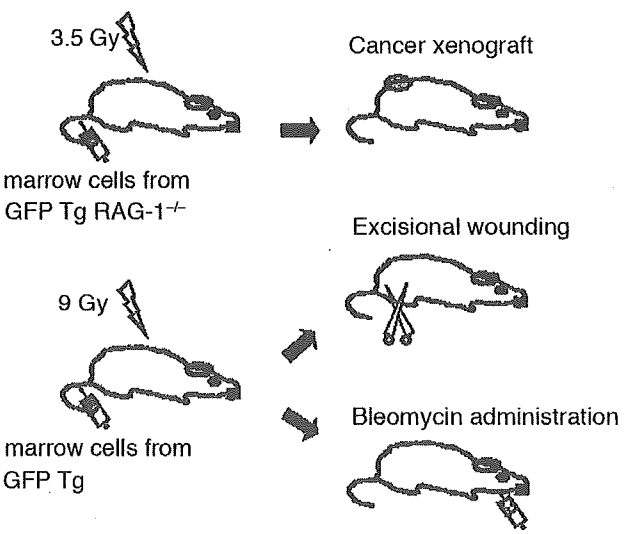

Figure 1. Protocol of mouse bone marrow transplantation and induction of fibrotic lesions. Marrow cells from green fluorescent protein (GFP) Tg and RAG-$1^{-/-}$ (GFP transgenic and recombination activating gene 1 knockout) mice were transplanted into irradiated (3.5 Gy) severe combined immunodeficient mice for cancer implantation. Marrow cells from GFP Tg mice were transplanted into irradiated (9 Gy) B6 mice for excisional wounding and bleomycin administration.

For creating fibrotic lesions induced by excisional wounding, we transplanted marrow cells from GFP Tg mice into irradiated (9 Gy) B6 mice. At 4 weeks after BMT, we cut the skin of the right thigh using a dispopunch (Maruho Co., Osaka, Japan). One week later, skin of the right thigh was resected and examined histologically. For control analysis, skin of the left thigh was also resected.

For creating fibrotic lesions induced by bleomycin administration, B6 mice transplanted with GFP Tg marrow cells were treated with endotracheal bleomycin (Nihon Kayaku, Tokyo, http://www.nipponkayaku.co.jp/english) 4 weeks after BMT. Briefly, bleomycin was dissolved in sterile saline at 3.3μg/ml. BMT mice were treated with 5 μg/g body weight of bleomycin or the same volume of saline only. Four weeks after treatment, the lungs were removed and histologically analyzed.

Immunohistochemical Analysis

Immunostaining was performed on 4-μm formalin-fixed, paraffin-embedded tissue sections. Sections were treated for 20 minutes using a microwave-based antigen-retrieval technique with 10 mmol/L citrate buffer, at pH 6.0 and 90°C. Endogenous peroxidases were inactivated with 3% H_2O_2 in methanol. Sections were incubated for 1 hour with rabbit polyclonal anti-GFP Ab (Molecular Probes, Eugene, OR, http://www.probes.com), then with the DAKO EnVision+System-HRP (Dako Cytomation, Glostrup, Denmark, http://www.dakocytomation.com). The reacted products were stained with diaminobenzidine.

Immunofluorescence and Confocal Microscopy

Paraffin-embedded specimens were cut into 4-μm thick sections. Sections were treated using either a microwave-based antigen-retrieval technique (for CD34, C-kit and α-SMA staining) or a proteinase K solution (Dako) for 10 minutes at room temperature (for collagen type I staining). When rat monoclonal antibodies were used, sections were blocked using the MOM immunodetection kit (Vector Laboratories, Burlingame, CA, http://www.vectorlabs.com). Sections were incubated with the primary antibodies, including rabbit polyclonal anti-GFP Alexa Fluor 488 (Molecular Probes) at a 1:500 dilution and rabbit polyclonal anti-collagen type I (Calbiochem, San Diego, http://www.emdbiosciences.com) at a 1:500 dilution; rat monoclonal anti-mouse CD34 (MEC14.7; HyCult Biotechnology, Uden, Netherlands, http://www.hbt.nl) at a 1:10 dilution; rabbit polyclonal anti-C-kit (Santa Cruz Biotechnology, Santa Cruz, CA, http://www.scbt.com) at a 1:100 dilution; and rabbit polyclonal anti-α-SMA (Lab Vision, Fremont, CA, http://www.labvision.com) at a 1:50 dilution. After washing the sections, either Alexa Fluor 546 goat anti-rat IgG or Alexa Fluor 546 goat anti-rabbit IgG (Molecular Probes) was used as the secondary antibody. Frozen sections were cut into 5-μm thick sections and were fixed in 10% formaldehyde for 5 minutes. Endogenous peroxidases were inactivated with 3% H_2O_2 in methanol. Sections were incubated with the primary antibodies, including rabbit polyclonal anti-GFP Alexa Fluor 488 at a 1:500 dilution; rat monoclonal anti-mouse CD45 (30-F11; eBioscience, San Diego, http://www.ebioscience.com) at a 1:200 dilution; and rat monoclonal anti-mouse Thy 1.2 (53-2.1, BD Bioscience, Franklin Lakes, NJ, http://www.bdbioscience.com) at a 1:50 dilution. After washing the sections, Alexa Fluor 546 goat anti-rat IgG was used as the secondary antibody. Before mounting, all sections were stained with DRAQ5 (Alexis Biochemical, Lausen, Switzerland, http://www.alexis-corp.com) for the discrimination of nucleated cells.

After mounting, the sections were examined using an LSM5 Pascal confocal imaging system (Carl Zeiss, Jena, Germany, http://www.zeiss.com). The sections were examined using an inverted microscope with an excitation wavelength of 488 nm for Alexa Fluor 488, 568 nm for Alexa Fluor 546, and 633 nm for DRAQ5. Confocal images were stored as digital files and viewed using Photoshop (Adobe, Mountain View, CA, http://www.adobe.com).

Laser Capture Microdissection and Reverse Transcription Polymerase Chain Reaction (RT-PCR)

To confirm the specificity of immunofluorescence with collagen type I, RT-PCR was performed on fibroblasts staining positive and negative for GFP using material obtained by the laser capture microdissection system (PixCell-II; Arcturus, Mountain View, CA, http://www.arctur.com). In brief, the dehydrated 10-μm frozen tissue section was overlaid with a thermoplastic membrane mounted on optically transparent caps, and GFP^+ and GFP^- fibroblasts (each corresponding to 500 to 1,000 cells) were captured by focal melting of the membrane through laser activation. The captured tissues were then immersed in denaturation Trizol solution (Life Technologies, Gaithersburg, MD, http://www.lifetech.com), and total RNA was extracted. RNA was redissolved in 10 μl of oligo$(dT)_{20}$ primer solution, and cDNAs were synthesized using the ThermoScript RT-PCR system (Life Technologies) in a final volume of 20 μl. One μl of cDNA solution was subjected to 40 PCR cycles of 10 seconds at 95°C, 10 seconds at 53°C–65°C, and 5–15 seconds at 72°C in a 10-μl mixture containing 2.25 mM $MgCl_2$ and 0.25 μM each of forward and reverse specific primers. The primer sequences were as follows:

Collagen type I: forward: 5'-CTACTCAGCCGTCTGTGCCT-3'; reverse: 5'-GGCAGG GCCAATGTCTAGT-3'
GFP: forward: 5'-AAGTTCATCTGCACCACCG-3'; reverse: 5'-TCCTTGAAGAAG ATGGTGCG-3'
GAPDH: forward: 5'-TTGAAGGTAGTTTCGTGGAT-3'; reverse: 5'-GAAAATCTG GCACCACACCTT-3'

Assessment of the Immunohistochemistry and Double Immunofluorescence Findings

The proportions of BM-derived fibroblasts were determined by the ratio of GFP^+ fibroblasts (GFP-Fbs) to the total number

of tissue fibroblasts. The fields for cell counting were randomly selected in each tissue of BMT mice ($n = 3$ or 4). At least 100 fibroblasts were counted in each high-power field (×400), and each numerical value was averaged. The proportion of both GFP and each fibroblast marker (CD34, C-kit, CD45, Thy-1, and α-SMA) fibroblasts to the total GFP-Fbs was analyzed by the overlay image of the three fluorescent images (GFP, fibroblast marker, and DRAQ5). At least 10 fields were randomly selected in each tissue for cell counting. At least 100 GFP-Fbs were counted in each high-power field (×400), and each numerical value was averaged. All data are presented as mean ± SEM. Comparison between groups was made using two-way analysis of variance. $p < .05$ was considered statistically significant.

Results

Recruitment of BM-Derived Fibroblasts into Noninjured Skin and Lung

Sublethally irradiated mice were injected with 1×10^7 GFP-labeled BM cells. GFP phenotyping of BM cells from the recipient mice demonstrated that their marrows had been reconstituted by high levels (>80%) of donor cells 4 weeks after BMT (data not shown). Since sublethal irradiation may induce sequential events of tissue damage, we first evaluated the effects of irradiation on the skin and lung of the BM chimera mice. Histological examination revealed essentially normal skin and lung architecture without fibrosis, although mild perivascular inflammatory cell infiltration was pointed out. Since we focused on fibroblasts as cells with pivotal roles in the fibrosis, BMT in the process of creating BM chimera mice had no significant effects on the morphological analysis of the fibrotic process of the skin and lung. An antibody specific for GFP was used to investigate whether fibroblasts were of BM origin. In the skin of BM chimera mice, GFP-Fbs were mainly found adjacent to striated muscle of the dermis (Fig. 2 A–C). The frequency of GFP-Fbs within the total skin fibroblast was 8.7% ± 4.6%. In the lung, GFP-Fbs were found located around the bronchus and the vessels within the bronchovascular bundle (Fig. 2 D–F). The frequency of GFP-Fbs was 8.9% ± 2.5 % (Table 1).

Increased Recruitment of BM-Derived Fibroblasts into Fibrotic Lesions Induced by Cancer Implantation and Excisional Wounding

After implantation of a transplantable human large cell neuroendocrine carcinoma of the lung into the skin, stromal fibrosis occurred prominently (Fig. 3A–B). Among the fibroblasts around the cancer nests, numerous fibroblasts showed positive reaction for GFP, and the frequency of GFP-Fbs was 59.7% ± 16.3% (Fig. 3C; Table 2). Upon excisional wounding, the injured area involving the deeper structure of the dermis and tissue was replaced by granulation tissue, which is comprised of many inflammatory cells and fibroblasts. Although GFP-Fbs were observed within the whole layer of skin, these cells have a tendency to locate in the deeper layer (Fig. 2 D–F). The frequency of GFP-Fbs per total fibroblasts was 32.2% ± 4.8%. In contrast, within lung fibrotic lesions induced by bleomycin administration, GFP^+ cells were mainly mononuclear cells without spindle cytoplasm, as shown in Figure 3I. The frequency of GFP-Fbs was 7.1% ± 2.4%, which was similar to the frequency found in control lung tissue.

BM-Derived Fibroblasts Expressed Collagen Type I

Deposition of collagen type I is a key characteristic finding in tissue fibrotic processes, and fibroblasts are a well-known major producer of this molecule. To determine whether GFP-Fbs express collagen type I and contribute to tissue fibrosis, sections from cancer implantation and excisional wounding were analyzed by confocal immunofluorescence microscopy. When germinal center B cells of the spleen in BMT mice were stained with GFP and type I collagen, numerous B cells showed positive for GFP, but type I collagen–positive cells were hardly observed (Fig. 4A). Any GFP^+ cells could not be detected in the mice reconsti-

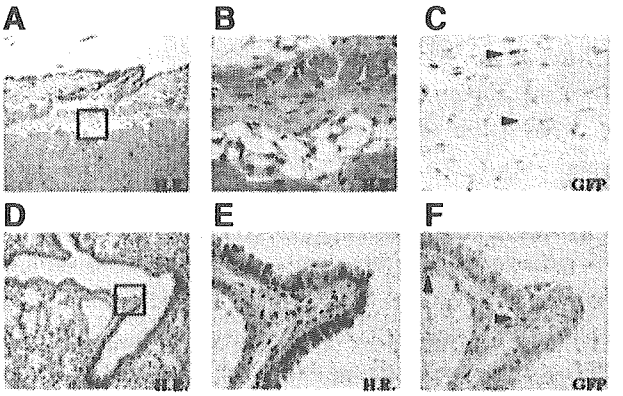

Figure 2. Microscopic appearance of **(A–C)** skin and **(D–F)** lung after bone marrow transplantation. Boxes indicate magnified regions of the **(A, B)** skin and **(D, E)** lung. **C** and **F** are serial sections of **B** and **E**, respectively. Arrowhead indicates GFP^+ fibroblasts. Abbreviations: GFP, green fluorescent protein; H.E., hematoxylin and eosin.

Table 1. Population (%) of green fluorescent protein–positive (GFP^+) fibroblasts

	% Population
Skin	
Noninjured	8.7 ± 4.6
Cancer implantation	59.7 ± 16.3[a]
Excisional wounding	32.2 ± 4.8[a]
Lung	
Saline	8.9 ± 2.5
Bleomycin	7.1 ± 2.4

Data are shown as the percentage of GFP^+ fibroblasts in whole fibroblasts of skin and lung. Data represent the mean ± SEM from three or four mice with bone marrow transplantation.
[a] $p < .01$.

tuted with GFP$^{-/-}$ (wild-type) marrow cells (Fig. 4B). As shown in Figure 4C–E, when GFP-Fbs were intermingled with GFP$^-$ fibroblasts within cancer implantation (Fig. 4C), excisional wounding (Fig. 4D), and noninjured skin (Fig. 4E), both GFP positive and negative fibroblasts expressed type I collagen. This phenomenon was further confirmed using microdissection analysis. Microdissected dermal fibroblasts of the mouse without BMT expressed type I collagen mRNA but did not express GFP mRNA (Fig. 4F, left lane). Microdissected GFP-Fbs around the cancer nests of BMT mice expressed both collagen type I and GFP mRNA (Fig. 4F, right lane). These results indicated that BM-derived fibroblasts produce type I collagen and contribute to tissue fibrosis.

Phenotype of BM-Derived Fibroblasts Within Fibrotic Lesions in the Skin

We assessed further phenotypes of GFP-Fbs with respect to their

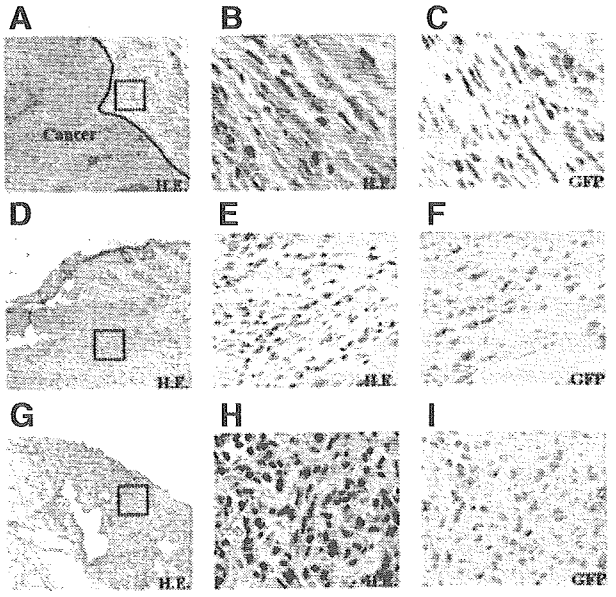

Figure 3. Microscopic appearance of skin and lung after **(A–C)** cancer implantation, **(D–F)** excisional wounding, and **(G–I)** bleomycin administration. Boxes indicate magnified regions of the skin after **(A, B)** cancer implantation, **(D, E)** excisional wounding, and **(G, H)** bleomycin administration. **C, F,** and **I** are serial sections of **B, E,** and **H,** respectively. Note that numerous GFP$^+$ fibroblasts are found in the fibrotic lesions induced by **(C)** cancer implantation and **(F)** excisional wounding, whereas few are found in **(I)** bleomycin administration. Abbreviation: H.E., hematoxylin and eosin.

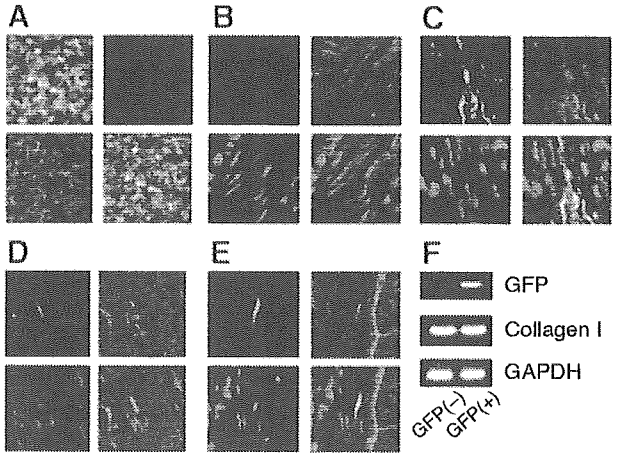

Figure 4. Colocalization of green fluorescent protein (GFP) and type I collagen on fibroblasts in the fibrotic lesions induced by cancer implantation and excisional wounding. **(A):** Germinal center B cells of the spleen in bone marrow–transplanted (GFP Tg) mice were stained with GFP and type I collagen. **(B):** Fibroblasts in cancer-induced stroma in the mice reconstituted with GFP$^{-/-}$ (wild-type) marrow cells were stained with GFP and type I collagen. **(C–E):** Fibroblasts in **(C)** cancer implantation, **(D)** excisional wounding, and **(E)** noninjured skin were stained with GFP and type I collagen. The upper left panel shows GFP fluorescence. The upper right panel shows cells immunostained with anti-type I collagen antibody in the same area. The lower left panel shows cells stained with DRAQ5 for the discrimination of nucleated cells. The lower right panel shows a composite of both fluorophores. **(F):** Reverse transcription polymerase chain reaction analysis of type I collagen gene in microdissected GFP$^+$ fibroblasts. GFP$^-$ fibroblasts also expressed type I collagen transcripts.

Table 2. Summary of phenotypes (%) of green fluorescent protein–positive (GFP$^+$) fibroblasts

	CD34	C-kit	CD45	Thy-1	α-SMA
Skin					
Noninjured	0±0	37.5±3.5	62.6±15.2	0±0	27.2±5.2
Cancer implantation	0±0	43.1±5.5	49.1±6.1	0±0	57.4±2.1[a]
Excisional wounding	0±0	38.5±6.3	46.7±2.8	0±0	28.3±5.0
Lung					
Saline	0±0	35.0±12.0	30.1±3.9	0±0	14.2±2.5
Bleomycin	0±0	43.4±11.8	34.2±10.0	0±0	18.3±5.8

Data are shown as the percentage of CD34$^+$, CD45$^+$, Thy-1$^+$, C-kit$^+$, and α-SMA$^+$ fibroblasts in GFP$^+$ fibroblasts. Data represent the mean ± SEM from three or four bone marrow chimera mice.

[a] $p = .002$

Abbreviation: α-SMA, α-smooth muscle actin.

potential identity with previously identified fibroblast phenotypes. Double immunofluorescence staining for GFP and fibroblast markers (including CD34, C-kit, CD45, Thy-1, and α-SMA) was performed with the sections from cancer implantation, excisional wounding, and noninjured skin. We could not determine any GFP$^+$/CD34$^+$ or GFP$^+$/C-kit$^+$ fibroblasts within the fibrotic lesions of the skin. As shown in Figure 5, some GFP-Fbs showed CD45, and these double-positive cells were intermingled with GFP$^+$/CD45$^-$ fibroblasts. The ratio of GFP$^+$/CD45$^+$ fibroblasts per GFP-Fb in the cancer-induced stroma and in the granulation tissue produced by excisional wounding was 43.1% ± 5.5% and 38.5% ± 6.3%, respectively (Fig. 5A, D). GFP-Fbs in noninjured skin also expressed CD45 in similar proportion (37.5% ± 3.5%) (Fig. 5G; Table 2). The cancer-induced stroma and granulation tissue induced by excisional wounding contained GFP$^+$/Thy-1$^+$ fibroblasts, and the frequency of double-positive cells per GFP-Fb was 49.1% ± 6.1% and 46.7% ± 2.8%, respectively (Fig. 5B, E). GFP$^+$/Thy-1$^+$ fibroblasts were also found in noninjured skin, and its frequency was 62.6% ± 15.2 % (Fig. 5H). The frequency of GFP$^+$/α-SMA$^+$ fibroblasts (BM-derived myofibroblasts) per GFP-Fb in the cancer-induced stroma was 57.4% ± 2.1%, and this frequency was significantly higher than that in noninjured skin (27.2% ± 5.2%; $p = .002$) (Fig. 5C, I; Table 2). To further confirm whether BM-derived fibroblasts express CD45 and Thy-1, we performed immunohistochemical staining for GFP/α-SMA/CD45, and GFP/α-SMA/Thy-1 in serial sections of cancer-induced stroma. In these sections, almost all spindle cells showed positive for both GFP and α-SMA, indicating that these cells are BM-derived myofibroblasts. Within this area, many CD45$^+$ spindle cells (Fig. 6A) and Thy-1$^+$ spindle cells (Fig. 6B) were observed. These results showed that BM-derived (myo)fibroblasts express CD45 and/or Thy-1.

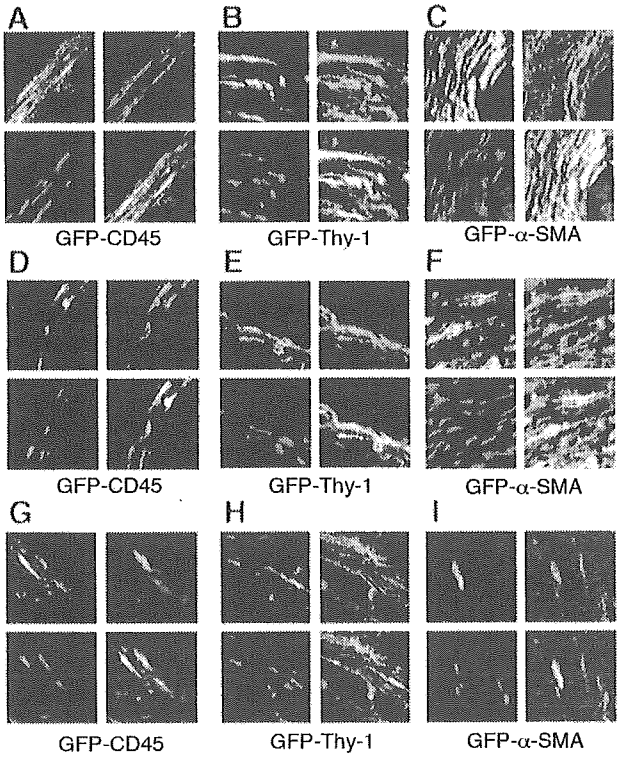

Figure 5. Colocalization of **(A, D, G)** green fluorescent protein (GFP)/CD45, **(B, E, H)** GFP/Thy-1, and **(C, F, I)** GFP/ α-smooth muscle actin (α-SMA) on fibroblasts in the fibrotic lesions induced by cancer implantation **(A–C)** and excisional wounding **(D–F)**, as well as **(G–I)** fibroblasts in noninjured skin. The upper left panel shows GFP fluorescence. The upper right panel shows cells immunostained with CD45, Thy-1, or α-SMA antibody in the same area. The lower left panel shows cells stained with DRAQ5 for the discrimination of nucleated cells. The lower right panel shows a composite of both fluorophores.

Discussion

Fibroblasts that enter and proliferate within fibrotic lesions had been thought to be of residual tissue origin; however, recent studies revealed that BM can be a source of fibroblast. The findings described by the previous reports and the current study could be a significant development toward understanding the potential effects of the BM-derived fibroblasts on the pathogenesis of tissue fibrosis. Controversy remains upon pulmonary fibrosis induced by bleomycin administration. Hashimoto et al. [29] reported that in the lung injury model induced by bleomycin, a significant number of BM-derived fibroblasts migrated into the fibrotic lesion in response to a factor released by lung injury. In contrast, we barely found a small number of GFP-Fbs (7.1% ± 2.4%), whereas many GFP$^+$ inflammatory cells existed in the fibrotic lesion. To confirm this result, we isolated and cultured fibroblasts from bleomycin-treated lung tissues, and the population of fibroblasts expressing GFP was examined by flow cytometry. The frequency of GFP$^+$ fibroblasts was about 7.3%, which was similar to the result found by immunohistochemical analysis. The reason for the discrepancy was unclear; however, the differences in the contribution of BM-derived fibroblasts might be caused by the different methods of irradiation or different doses of drugs.

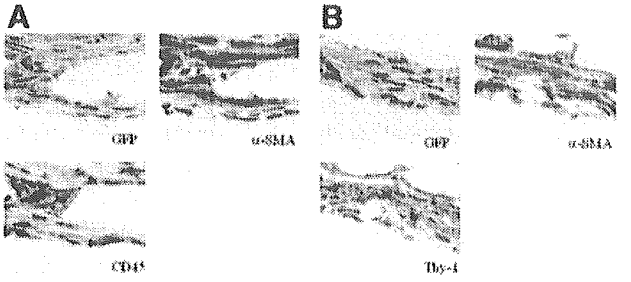

Figure 6. Immunohistochemical detection of CD45$^+$ bone marrow (BM)–derived fibroblasts and Thy-1$^+$ BM-derived fibroblasts. **(A):** Green fluorescent protein (GFP), alpha-smooth muscle actin (α-SMA), and CD45 staining of serial sections of cancer-induced stroma. **(B):** GFP, α-SMA, and Thy-1 staining of serial sections of cancer-induced stroma.

As fibroblast is a key producer of collagen and has a central role in tissue fibrosis, we examined whether BM-derived fibroblasts also produce type I collagen. Almost all of the BM-derived fibroblasts within a fibrotic lesion induced by cancer implantation and excisional wounding expressed type I collagen (Fig. 4A, B). Considering the fact that significant numbers of BM-derived fibroblasts were present within the cancer stroma (59.7% ± 16.3%) and wound healing tissue (32.2% ± 4.8%), these results argue for the major direct role for these cells in the process of pathological fibrosis.

To define the further phenotypic signatures of BM-derived fibroblasts in vivo, we performed double immunofluorescence analysis. It should be noted that GFP-Fbs within both fibrotic lesion and dermis of the noninjured skin expressed in varying degrees of CD45, Thy-1, and α-SMA, indicating BM-derived fibroblasts were heterogenous with respect to phenotypic features. Although CD45 has been considered to be a lineage-restricted pan-hematopoietic marker [31, 32] and $CD45^+$ mouse marrow stromal cells could not be detected in vitro culture in our preliminary experiment (data not shown), recent study showed that human BM mesenchymal cells expressed CD45 in vivo and were dramatically downregulated by in vitro culture [33]. Singer et al. [34] reported that the BM stromal cell line generated by SV-40 transformation expressed hematopoietic markers, including CD45. In the current study, the frequency of $CD45^+$ fibroblasts per GFP^- fibroblast was 29.2% ± 0.6% (data not shown), whereas the frequency of $CD45^+$ fibroblasts per GFP-Fb within cancer stroma and wound-healing tissue was 52.9% ± 15.9% and 66.1% ± 3.9%, respectively. Therefore, given that mesenchymal stem cells are the source of BM-derived fibroblasts, CD45 might be a candidate marker of BM-derived fibroblasts in this model. Furthermore, the presence of a significant proportion of $CD45^-$ BM-derived fibroblasts would be explained by the possibility that BM-derived fibroblasts are of heterogenous origin or that CD45 might be downregulated within fibrotic microenvironments.

Thy-1 is a cell-surface glycoprotein, whose function remains ill-defined. Human fibroblasts were heterogeneous with respect to surface Thy-1 expression [35–37]. $Thy\text{-}1^+$ and $Thy\text{-}1^-$ subsets showed functionally distinct subpopulations in inflammatory cytokine production, prostaglandin production, CD40 expression [35, 36], and lineage differentiation [37], suggesting that the balance between these populations might contribute to tissue homeostasis. We investigated whether BM-derived fibroblasts within fibrotic lesions belong to either the $Thy\text{-}1^+$ or the $Thy\text{-}1^-$ subpopulation. We found, however, that BM-derived fibroblasts comprised both $Thy\text{-}1^+$ and $Thy\text{-}1^-$ subpopulations to the same degree. Therefore, BM-derived fibroblasts are phenotypically heterogeneous with respect to the Thy-1 expression, which may have important consequences in the pathogenesis of fibrotic process.

A subpopulation of fibroblasts has been reported to express α-SMA, and these cells are called myofibroblasts. Myofibroblasts have been observed in normal and pathological situations and are considered responsible for the contractile forces that close wound margins. The frequency of $GFP^+/\alpha\text{-}SMA^+$ per GFP-Fb within cancer-induced stroma was 59.3% ± 2.0%, and this frequency was significantly higher than that found within the dermis of nonfibrotic skin (37.4% ± 8.5%). In our data, the proportion of $\alpha\text{-}SMA^+$ fibroblasts was variable and depended on the cancer characteristics (unpublished data). This phenomenon might be explained by the persistent provision of mediators such as transforming growth factor–beta and tumor necrosis factor-α secreted by cancer cells, which are implicated in maintaining myofibroblast formation.

Early studies described the presence of fibroblasts in normal peripheral blood, termed circulating fibrocytes. Circulating fibrocytes comprise 0.1%–0.5% of the human nonerythrocytic cell population in peripheral blood [38, 39]. Thus it is possible to speculate that BM-derived fibroblasts are identical with the population of circulating fibrocytes. However, the results obtained here revealed that BM-derived fibroblasts and circulating fibrocytes showed different phenotypes, since circulating fibrocytes express both CD45 and CD34, whereas BM-derived fibroblasts in our model express CD45 but not CD34. Furthermore, previous reports described that when using sex-mismatched BM chimera mice, circulating fibrocytes originated from the host tissue, not from transplanted marrow cells. It would be interesting to examine whether BM-derived fibroblasts and circulating fibrocytes are from the same source.

The results that GFP-Fbs could also be found in subcutaneous tissue of noninjured skin and lung suggested that BM can potentially contribute to the turnover of fibroblasts and are involved in tissue homeostasis. However, it must be kept in mind that this occurred in the context of sublethal irradiation and BMT.

Increased research on fibroblasts has made clearer the concept of subset specialization of fibroblasts. Further studies about the phenotypical and functional analyses of BM-derived fibroblasts would help us gain insight into the pathogenesis of the fibrotic process.

ACKNOWLEDGMENTS

We are grateful to Yoko Okuhara and Chie Okumura for technical support and Suzaki Motoko for help in preparing the manuscript. This work was supported in part by the Grant-in-Aid for Cancer Research from the Ministry of Health, Labour and Welfare; the Grant for Scientific Research Expenses for Health Labour and Welfare Programs; the Foundation for the Promotion of Cancer Research, 2nd-Term Comprehensive 10-Year Strategy for Cancer Control; and Special Coordination Funds for Promoting Science and Technology from the Ministry of Education, Culture, Sports, Science and Technology, the Japanese Government. T.S. is a recipient of Research Resident Fellowships from the Foundation for Promotion of Cancer Research.